3-26-2015

Pilot Assisted Inertial Navigation System Aiding Using Bearings-Only Measurements Taken Over Time

Anthony T. Mirabile

PILOT-ASSISTED INERTIAL NAVIGATION SYSTEM AIDING USING BEARINGS-ONLY MEASUREMENTS TAKEN OVER TIME

THESIS

Anthony T. Mirabile, 1st Lieutenant, USAF

AFIT-ENG-MS-15-M-015

DEPARTMENT OF THE AIR FORCE
AIR UNIVERSITY

AIR FORCE INSTITUTE OF TECHNOLOGY

Wright-Patterson Air Force Base, Ohio

AFIT-ENG-MS-15-M-015

PILOT-ASSISTED INERTIAL NAVIGATION SYSTEM AIDING USING BEARINGS-ONLY MEASUREMENTS TAKEN OVER TIME

THESIS

Presented to the Faculty

Department of Electrical and Computer Engineering

Graduate School of Engineering and Management

Air Force Institute of Technology

Air University

Air Education and Training Command

in Partial Fulfillment of the Requirements for the

Degree of Master of Science in Electrical Engineering

Anthony T. Mirabile, B.S.E.E.

1st Lieutenant, USAF

March 2015

AFIT-ENG-MS-15-M-015

PILOT-ASSISTED INERTIAL NAVIGATION SYSTEM AIDING USING BEARINGS-ONLY MEASUREMENTS TAKEN OVER TIME

THESIS

Anthony T. Mirabile, B.S.E.E.
1st Lieutenant, USAF

Committee Membership:

Dr. Meir Pachter
Chair

Dr. Kyle J. Kauffman
Member

Dr. John F. Raquet
Member

Abstract

The objective of this work is to develop an alternative Inertial Navigation System (INS) aiding source other than the Global Positioning System (GPS) while preserving the autonomy of the integrated navigation system. It is proposed to develop a modernized method of aerial navigation using driftmeter measurements. Use of an Electro-Optical (E/O) system (LANTIRN or Sniper) for ground feature tracking by the pilot, and an independent altitude sensor (baro altimeter or radar altimeter) in conjunction with the INS, is envisioned. The idea is to use measurements taken by the pilot using the E/O system to aid an existing INS, thus automating the navigator's function. The pilot will track a ground feature with the E/O system, while the aircraft is on autopilot holding constant airspeed, altitude, and heading during an INS aiding session. The ground feature measurements from the E/O system and the INS output will be used to form measurements provided to a linear Kalman Filter (KF) running on the navigation computer to accomplish the INS aiding action. Aiding the INS will be periodically repeated as operationally permissible under pilot discretion. The structured environment: constant speed, constant altitude, and wings level flight while on autopilot justifies the linearization of the KF kinematic and measurement equations used during an INS aiding session. Due to justified linearization conditions, little to no modeling error will be present when implementing a linear Kalman filter. Therefore, the strength of the INS aiding action will be exclusively determined by the prevailing degree of observability. It is shown that after one short aiding period a 60% reduction in position covariance is realized.

AFIT-ENG-MS-15-M-015

My thesis is dedicated to all who have positively impacted my life, preparing me for the rigor associated with a technical masters. Family, friends, and mentors who have made an impression on me, thank you.

Acknowledgements

Special recognition to my advisor, Dr. Meir Pachter for all his extra hours spent explaining concepts and helping me to knock down roadblocks. My committee members, Dr. Kyle Kauffman and Dr. John Raquet provided me with research guidance and perspective, along with valuable skills necessary to accomplish this research from my time in their classroom. The students in the GNC track at AFIT, our long technical discussions over coffee or a rip it will be some of my fondest memories from this research experience.

Table of Contents

Page

List of Figures

List of Tables

PILOT-ASSISTED INERTIAL NAVIGATION SYSTEM AIDING
USING BEARINGS-ONLY MEASUREMENTS TAKEN OVER TIME

I. Introduction

1.1 Motivation

Since the wide-spread use of the GPS in military applications, alternate sources of precision navigation were effectively neglected due to the accuracy and technology development associated with GPS integration. The dependence on GPS was driven by the precision and reliability observed in multi-faceted military applications. As the first nation to design, manufacture, and proliferate a Global Navigation Satellite System (GNSS), we have been afforded unparalleled navigation and timing capabilities never before seen in the world. Satisfying precision navigation requirements for ground, flight, and sea based missions spawned the integration and improvement of GPS technology into virtually all applicable military technologies.

The ease associated with GPS receiver integration for precise timing and navigation has become a hidden standard for technology development in military and civilian applications. Pushing all in on GPS technology for navigation, coupled with technology development saturation in support of the War on Terror, the United States military recognizes the need to establish an alternate precision navigation source. The challenge is evident when comparing navigation accuracy solutions to GPS, along with a source as environmentally robust as GPS.

With the high volume product use of GPS technology in military applications, senior leaders identified the need to explore alternative precision navigation technolo-

gies other than GPS. Former Secretary of the Air Force General Norton A. Schwartz advocated for the reduction of dependence in GPS in 2010 at the Fletcher Conference on National Security Strategy and Policy: "It seems critical, to me, that the Joint Force should reduce its dependence on GPS-aided precision navigation and timing, allowing it to ultimately become less vulnerable, yet equally precise, and more resilient" [20]. The active sensor nature of GPS lends itself to challenges including spoofing, jamming, and coverage outages. Spoofing or jamming of the GPS signal is a feasible concern adversaries have the ability to exploit. However, the fidelity and robustness of military GPS does provide degrees of protection against spoofing and jamming in specific conditions. Aside from hostile navigation interference, receive availability of the GPS signal is either constrained or not possible when under cover (bridges, caves, trees, etc.) and in crowded Radio Frequency (RF) reflective environments like cities or urban environments where multi-path errors are increased. Therefore, much inspiration has been drawn from biological inspired navigation. Inspired from human vision, the passive nature of an Electro-Optical (E/O) system is advantageous to explore as an alternative inertial aiding source. Going back to the classical navigation equipment, the self contained INS, coupled with biological inspired navigation has become a growing research field striving for an alternative precision navigation source independent of GPS [6].

There has been a strong navigation community movement towards vision-aided navigation with the improvement in sensing capabilities, and decreased size, weight, power, and cost constrains associated with inertial systems. The vision aided navigation problem begins with the use of a passive E/O (Electro-Optical) sensor to track features in the scene to aid an inertial system. The elements of these research efforts strongly hinge on the ability for computer vision algorithms to identify and track distinct features in the scene. However, there are still a multitude of research

opportunities on the filtering and modeling aspects of the problem, specifically with the INS. Success has been made with feature based tracking for inertial system aiding using stochastic projection in a tightly coupled implementation for navigation [24] where Monte Carlo simulations were run prior to experimental testing with a binocular vision system aiding a tactical and consumer grade Inertial Measurement Unit (IMU).

During World War II aircraft like the B-17 and B-24 were equipped with a sighting device operated by the navigators known as the driftmeter. Sitting in the glazed nose of the aircraft using the dirftmeter, the navigator was able to calculate the ground speed and the wind vector. In a time where navigation using dead reckoning or pilotage were the main options, the driftmeter was a revolutionary navigation device. Further technical explanation of the driftmeter will be presented in Chapter II.

Inertial systems installed and operating on aircraft are susceptible to an accumulation of errors over time and require an update source for precision navigation. In the event, GPS is not available to provide inertial system updates, a common practice is Initial Point (IP) updates. Surveyed landmarks are logged in memory prior to flight and the pilot must overfly these points, and conduct an absolute inertial system update. The nature of IP updates can lead to unquantified bias errors varying between pilots as the IP update is conducted based on a visual flyover. Also, pilots are constrained to the surveyed landmarks pre-loaded for absolute IP updates. Allowing the pilot navigation freedom in a setting where GPS is not available and IP updates are not possible is the goal. Herein lies the motivation for this research effort; can a pilot track an arbitrary ground feature to gain a relative inertial system update improving the navigation solution.

Investigating the strength of the aiding action driftmeter operators were able to provide serves as the starting point for this research. In the process of replicating

driftmeter operations, an interesting subject of observability through correlation was uncovered. Where observability is a deterministic control system concept and correlation is a stochastic modeling concept. Knowing that the system dynamics is the link between observability and correlation for a linear system, this research pushes to understand the benefits available from the gained observability.

1.2 Thesis Organization

Here in Chapter I, the introduction, a basic overview of the motivation is presented as contextual grounds for the reminder of the document. Chapter II covers the background concepts necessary to understand the research along with the literature review. In Chapter III, the methodology used to construct simulation and analysis is outlined. Results and analysis of simulations are covered in Chapter IV. Lastly, Chapter V draws conclusions and provides insight on future research extensions and applications.

II. Mathematical Background

In this chapter, a detailed overview of the mathematics and physics relating to vision aided inertial navigation will be presented. Understanding or familiarity with the concepts presented will enable comprehension of the inertial navigation research covered here within.

2.1 Notation

For convention purposes, the following are a list and explanation of mathematical notation used in this thesis.

Scalars: upper or lower case italicized letters, (e.g., k or K).

Vectors: lower case bold letters or symbols, (e.g., $\mathbf{a}$). All vectors referenced will be column vectors with $\mathbf{a}_{(i)}$ being the element in the i$^{\text{th}}$ row of the column vector $\mathbf{a}$.

Matrices: upper case letters or symbols in bold font (e.g., $\mathbf{X}$). $\mathbf{X}_{t(i,j)}$ is the scalar element of the i^{th} row and the j^{th} column of the matrix $\mathbf{X}$ and t is the associated time.

Transpose: transpose of a vector or matrix will be defined with the superscript T (e.g., $\mathbf{a}^{\mathrm{T}}$ or $\mathbf{X}^{\mathrm{T}}$).

Estimated Variables: estimates of random variables, vectors, or matrices, will be identified with the *hat* character (e.g., $\hat{x}, \hat{\mathbf{a}}, \hat{\mathbf{X}}$).

Calculated Variables: variables, vectors, or matrices, computed which contain errors will be identified with the *tilde* character (e.g., $\tilde{x}, \tilde{\mathbf{a}}, \tilde{\mathbf{X}}$)

Measured Variables: variables measured which contain errors will be identified with the *bar* character (e.g.,$\bar{x}, \bar{\mathbf{a}}, \bar{\mathbf{X}}$)

Direction Cosine Matrix (DCM): a transformation from frame a to frame b is denoted by $\mathbf{C}_a^b$

Reference Frame: the reference frame a vector is referenced in will be denoted by a superscript letter in parentheses, describing the reference frame (e.g., $\mathbf{a}^{(\mathrm{b})}$ where vector $\mathbf{a}$ is expressed in the b-frame). Reference frame axes will be defined with the axis as a lower case letter with the reference frame annotated as a subscript (e.g., x_b defining the body frame's x axis)

Relative Motion: relative motion between two different frames will be denoted by the subscripts of both reference frames, read from right to left (e.g., ω_{ab} is the rotation rate of the b-frame relative to the a-frame).

Time: time will be identifiable in vectors or matrices in both continuous and discrete time. Continuous time will be designated as the first subscript of either a matrix, vector, or scalar (e.g., $\mathbf{a}(t), \mathbf{A}(t)$). Discrete time will be designated with a subscript of the time index (e.g., $\mathbf{x}_t, \mathbf{P}_t$).

2.2 Coordinate Reference Frames

Navigation is fundamentally based around the concept of reference frames. Reference frames define a convention to organize and account for all necessary physical motion to utilize sensor information. A multitude of reference frames have been defined over the years. The true inertial frame, Earth-fixed inertial frame, Earth centered Earth fixed frame, Earth-fixed navigation frame, and the body frame typically encompass the reference frames used in inertial navigation.

True Inertial Frame.

The true inertial frame is a theoretical non-rotating, non-accelerating reference frame where Newton's laws apply. With no predefined origin or orientation, the true inertial frame is a conceptual reference frame.

Earth-fixed Inertial Frame.

The Earth-fixed inertial frame originates at the center of the earth with three non-rotating orthogonal axes in respect to the stars. Axis $\mathbf{z}_i$ aligns with Earth's polar axis and $\mathbf{x}_i$ aligns with the equator and points to the first star of Aries. The $\mathbf{y}_i$ axis is the complement of the $\mathbf{x}_i$ and $\mathbf{z}_i$ axes maintaining an orthogonal right hand rule coordinate frame. Properties of navigation in the Earth-fixed inertial frame are bound by Sir Issac Newton's Second Law of Motion $\mathbf{F} = m \cdot \mathbf{a}$. Where $\mathbf{F}$ is the force with units $N = \frac{kg\ m}{s^2}$, m is the mass of the body, and $\mathbf{a}$ is the acceleration of the body. Therefore, physical laws of motion apply and proves to be necessary in inertial navigation.

Earth Centered Earth Fixed Frame.

The Earth Centered Earth Fixed frame's orthogonal axes are fixed based on the Earth. The $\mathbf{z}_e$ axis aligns with Earth's polar axis like the Inertial Frame, and the $\mathbf{x}_e$ axis aligns with the equator and 0° longitude. Satisfying orthogonal properties and the right hand rule, the $\mathbf{y}_e$ axis also passes through the equatorial plane as the orthogonal complement of the $\mathbf{x}_e$ and $\mathbf{z}_e$ axes. The Earth Centered Earth Fixed (ECEF) frame rotates with respect to the inertial frame about the $\mathbf{z}_e$ axis at a rate of $\omega_{\text{ie}} = 360°/23\text{hr } 56\text{min}$.

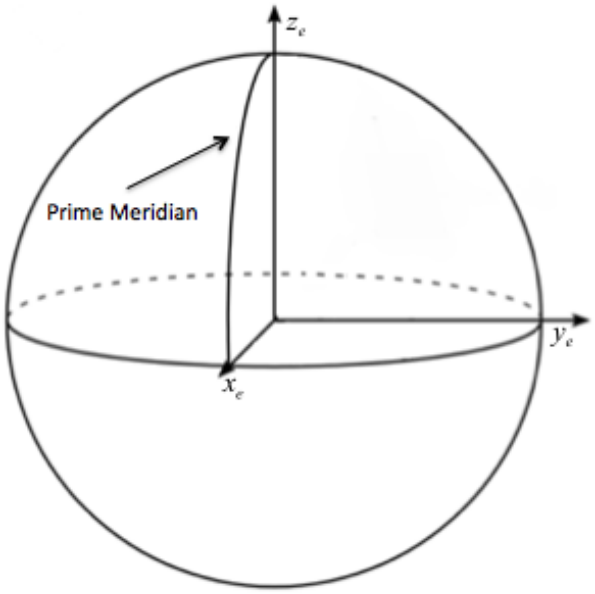

Figure 1. Earth Centered Earth Fixed Frame

Earth-Fixed Navigation Frame.

Also known as the local level frame, the Earth-fixed navigation frame designates an origin at the location of the vehicle with a right hand rule convention with the $\mathbf{z}_n$ axis perpendicular to the earths surface. Unlike the inertial frame and the ECEF frame, the navigation frame changes as vehicle position changes. Navigating with the navigation reference frame requires knowledge of the Earth rotating. The transport rate is dependent on the location of the vehicle with respect to the turn rate of the Earth centered Earth fixed frame (ω_{en}).

Utilized in this research as the Earth-fixed navigation frame, satisfying the right hand rule, is an East - North - Up (ENU) convention which can be seen in Figure 2.

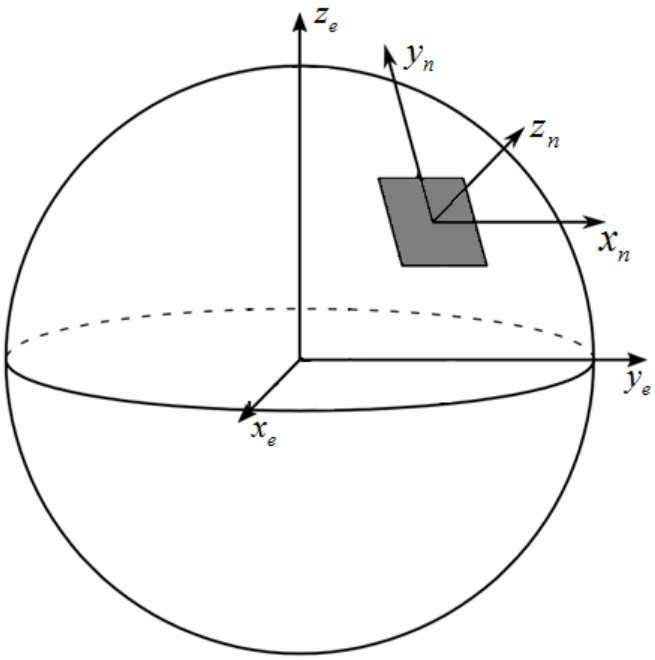

Figure 2. East North Up Navigation Reference Frame

Body Frame.

The body frame is utilized for vehicle measurements and is dependent on the mounting orientation of the sensors on the vehicle. In a strapdown INS system, the body frame measurements will need to be transformed to the selected navigation reference frame to for correct incorporation of sensor measurements. A diagram of the ENU body frame is depicted in Figure 3 where $\mathbf{x}_b$ is the axis pointing out the front of the aircraft nose, $\mathbf{y}_b$ orthogonally points out the left wing, and $\mathbf{z}_b$ is the up direction. The origin of this coordinate frame is the location of the sensor cluster. If the sensor cluster is not co-located at the center of gravity of the aircraft, the measurement lever arm must be handled.

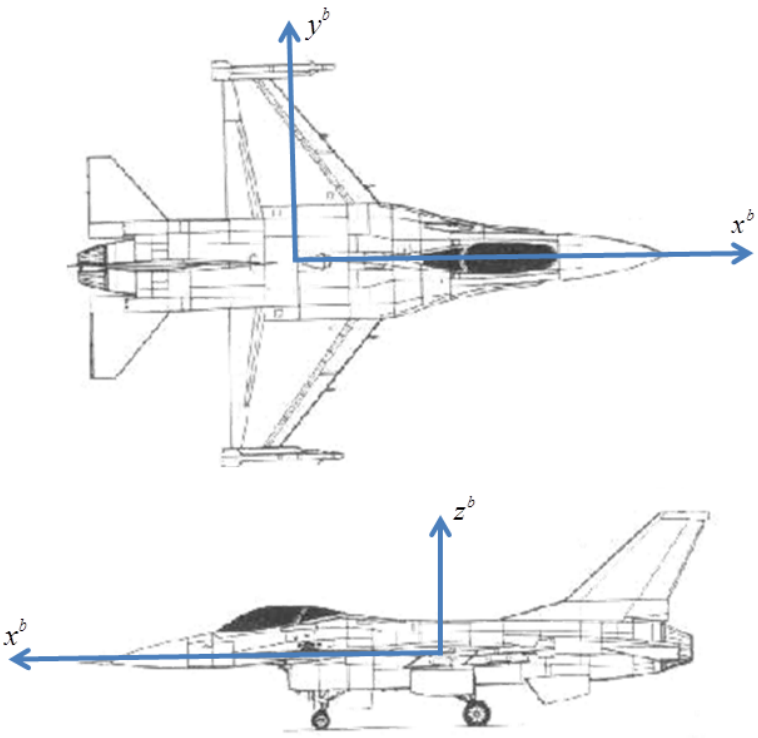

Figure 3. Aircraft Body Frame

Camera Frame.

An E/O system is used specifically in this research but essentially, a camera is considered. The camera frame is located at the optical center of the camera which is rigidly attached to the body of the aircraft for the purposes of this inertial navigation research. Therefore, the camera frame is co-located with the body frame and no DCM or lever arm is necessary when using E/O system measurements. Camera frame coordinate axes are defined with the $\mathbf{z}_c$ pointing straight out from the optical center of camera, and $\mathbf{x}_c$ pointing up, and $\mathbf{y}_c$ pointing to the left from the vantage point of the optical center to the scene. The camera frame is where the projection of the image in the scene will be resolved for measurements.

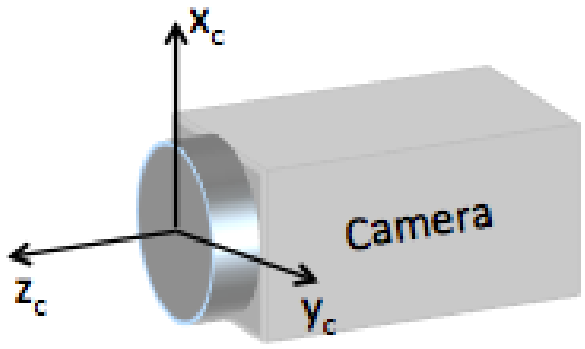

Figure 4. Camera Frame

2.3 Coordinate Transformations

Coordinate transformations allow measurements in one reference frame to be utilized in another reference frame. Vector transformation operations are accomplished with a matrix capturing the relationship between the two frames of reference. The process of transforming information between coordinate frames can be accomplished with a few techniques. Direction Cosine Matrices, Quaternions, and Euler angle rotations all can be implemented to perform a transformation of information between frames. Each have different implementations along with performance qualities.

Euler Angle Rotations.

Euler angles are obtained as a sequence of three rotations performed in a specific order on an individual axis. The convention of rotations is (3,2,1) which indicates the first rotation is about the $\mathbf{z}_b$ axis, the second rotation about the $\mathbf{y}_b$ axis and the last rotation about the $\mathbf{x}_b$ axis. Individual rotations about each specific orthogonal axis can be seen in Equation (2.3). Euler angle rotations are a three parameter transformation with singularities existing at elevation angles $\pm 90^\circ$ [21].

$$\text{rotation } \psi \text{ about } \mathbf{z}_b\text{-axis}, \quad \mathbf{C}_1 = \begin{bmatrix} \cos\psi & -\sin\psi & 0 \\ \sin\psi & \cos\psi & 0 \\ 0 & 0 & 1 \end{bmatrix}$$

$$\text{rotation } \theta \text{ about } \mathbf{y}_b\text{-axis}, \quad \mathbf{C}_2 = \begin{bmatrix} \cos\theta & 0 & \sin\theta \\ 0 & 1 & 0 \\ -\sin\theta & 0 & \cos\theta \end{bmatrix}$$

$$\text{rotation } \phi \text{ about } \mathbf{x}_b\text{-axis}, \quad \mathbf{C}_3 = \begin{bmatrix} 1 & 0 & 0 \\ 0 & \cos\phi & -\sin\phi \\ 0 & \sin\phi & \cos\phi \end{bmatrix}$$

Combining the individual Euler angle axis rotations in the (3,2,1) convention yields the DCM $\mathbf{C}_b^n$ which rotates the body frame to the navigation frame.

$$\mathbf{C}_b^n = \mathbf{C}_1 \cdot \mathbf{C}_2 \cdot \mathbf{C}_3 \tag{1}$$

Expanding Equation (1) shows the relationship between each body frame and navigation frame axis. The full $\mathbf{C}_b^n$ expanded is

$$\mathbf{C}_b^n = \begin{bmatrix} \cos\theta\cos\psi & -\cos\phi\sin\psi + \sin\phi\sin\theta\cos\psi & \sin\phi\sin\psi + \cos\phi\sin\theta\cos\psi \\ \cos\theta\sin\psi & \cos\phi\cos\psi + \sin\phi\sin\theta\sin\psi & -\sin\phi\cos\psi + \cos\phi\sin\theta\sin\psi \\ -\sin\theta & \sin\phi\cos\theta & \cos\phi\cos\theta \end{bmatrix} \tag{2}$$

where each element in the matrix represents the cosine between the specific coordinate frame axes.

Simplification of Equation (2) due to small Euler angles is validly invoked in this research due to wings level, heading hold flight, and an East direction of flight. That

is, $(\psi, \theta, \phi)^T$ = small angles. Combining each Euler angle rotation generates a DCM. Because of small Euler angle assumptions, the expanded Euler angle rotation matrix, DCM, necessary to rotate the body frame to the navigation frame becomes Equation (3).

$$\mathbf{C}_b^n \approx \begin{bmatrix} 1 & -\psi & \theta \\ \psi & 1 & -\phi \\ -\theta & \phi & 1 \end{bmatrix} \tag{3}$$

Direction Cosine Matrix.

The Direction Cosine Matrix is a 3×3 matrix performing four parameter transformations which eliminate singularity concerns. Each element of the DCM shown in Equation (4) is equal to the cosine of the angle included between the orthogonal basis unit vectors of the original reference frame and the target reference frame.

$$\mathbf{C}_b^n = \begin{bmatrix} c_{11} & c_{12} & c_{13} \\ c_{21} & c_{22} & c_{23} \\ c_{31} & c_{32} & c_{33} \end{bmatrix} \tag{4}$$

Figure 5 shows the cosine of the angle between two corresponding reference frame axes which makes up an element of the DCM.

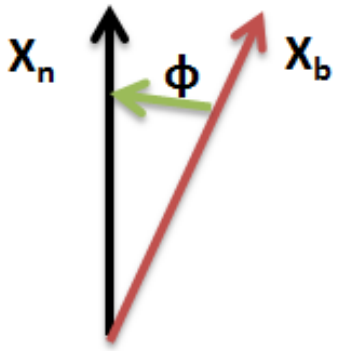

Figure 5. DCM Element Cosine Between Axes

An example implementation of DCMs can be seen in Equation (5).

$$\mathbf{a}^{(n)} = \mathbf{C}_b^n \mathbf{a}^{(b)} \tag{5}$$

Where vector $\mathbf{a}^{(b)}$ resides in the body frame and vector $\mathbf{a}^{(n)}$ resides in the navigation frame. The DCM $\mathbf{C}_b^n$ rotates the information in vector $\mathbf{a}^{(b)}$ to the navigation reference frame yielding $\mathbf{a}^{(n)}$. An important orthonormal property of DCMs exists:

$$\mathbf{C}_b^n \mathbf{C}_b^{nT} = \mathbf{C}_b^n \mathbf{C}_n^b = \mathbf{I} \tag{6}$$

Direction Cosine Matricies will mainly be used becuase of the absence of singularities, compared to Euler angle rotations.

Quaternions.

Quaternions are also a four parameter coordinate transformation like a DCM transformation, containing no singularities. The quaternion $\mathbf{q}$ is a quadruple, shown in Equation (7) where the four components are referred to as Euler's symmetric parameters which are constrained via Equation (8).

$$\mathbf{q} = \begin{pmatrix} q_1 \\ q_2 \\ q_3 \\ q_4 \end{pmatrix} \tag{7}$$

$$q_1^2 + q_2^2 + q_3^2 + q_4^2 = 1 \tag{8}$$

The relationship between coordinate frames is characterized based on a single rotation about a vector ϕ where α, β, γ are the angles between the reference axes and the axis of rotation ϕ [21]. A quaternion rotation vector is expressed by one real value and three imaginary values to perform the transformation.

$$\begin{pmatrix} q_1 \\ q_2 \\ q_3 \\ q_4 \end{pmatrix} = \begin{pmatrix} \cos\frac{\phi}{2} \\ \sin\frac{\phi}{2}\cos\alpha \\ \sin\frac{\phi}{2}\cos\beta \\ \sin\frac{\phi}{2}\cos\gamma \end{pmatrix} \tag{9}$$

2.4 Inertial Navigation

Inertial navigation systems operate within the laws of classical physical mechanics mathematically describing motion. Given technology has enabled the measurement of the normal force produced from a body's acceleration force, mathematical integration yields a calculation of changes in velocity and position over the measurement frequency of the sensor. A three-axis strapdown inertial navigation system will contain a minimum of three orthogonally mounted accelerometers measuring specific force, and three orthogonally mounted gyroscopes measuring angular rate. An important concept in inertial navigation is resolving the sensor measurements in the navigation frame of reference, referred to as mechanization.

The self contained nature of an inertial navigation system increases the degree of robustness to outside interference, compared to other navigation systems dependent on transmission of external signals. However, the challenges associated with inertial navigation systems come in the form of accumulation of errors. Over long flight intervals without aiding, INS errors can render the INS virtually useless for precision navigation. The ability to model the errors of the INS become paramount when using an external sensor, like an E/O system, to aid an INS.

Accelerometers.

Accelerometers measure translational motion with respect to inertial space. In the past, accelerometers were strictly mechanical devices. Recent rapid development of Micro-Electrical Mechanical Sensors (MEMS) technology has yet to show similar accuracy and precision as the mechanical accelerometers for use in navigation quality inertial systems. But, is certainly a growing field of research and has made significant developments in the consumer grade inertial. The cost associated with MEMS devices makes them advantageous in situations where degrees of navigation precision can be sacrificed, but the majority of applications use MEMS accelerometers and rate gyroscopes for control system feedback rather than navigation.

Measurements from an accelerometer measure total or specific force which includes a gravitational component, not just the acceleration of the body. A breakdown of Sir Issac Newton's Second Law of Motion in terms of what an accelerometer measures is shown in Equation (10), where g is the force due to gravity, a is the acceleration force of the body, and m is the mass of the body.

$$\begin{aligned} F &= \mathrm{m}a \\ F &= \mathrm{m}(a+g) \end{aligned} \tag{10}$$

Therefore, the gravitational component must be subtracted out of accelerometer measurements. Because gravity is not uniform all over the Earth, physical position must be used to calculate the force of gravity. Gravity models can be used to calculate the force of gravity at a physical location on Earth [5]. After the gravity is subtracted out from the specific force, the remaining force less the gravity model errors is the acceleration of the body.

A simple accelerometer model is shown in Figure 6 where an acceleration along the sensitive axis will cause the proof mass to move in the opposite direction, measuring specific force.

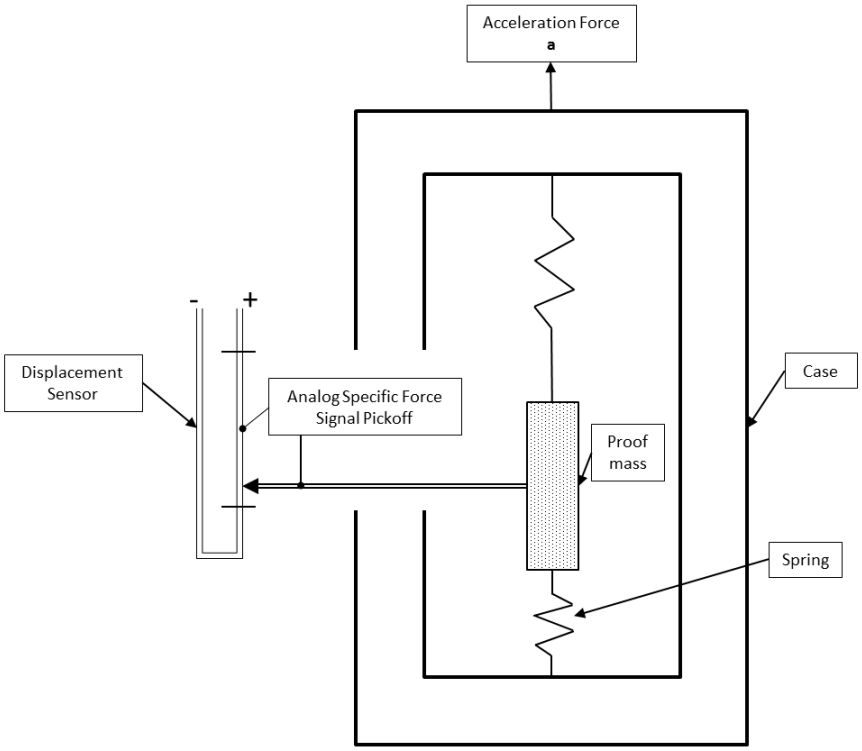

Figure 6. Simple Accelerometer Diagram

Gyroscopes.

Navigation gyroscopic sensors are used to measure changes in angular rate in order to resolve attitude in the navigation reference frame. Gyroscopes are critical to the

determination of the body to navigation frame coordinate transformation. Figure 7 shows a diagram of a 2-axis gimbaled gyro, which is different than a strapdown system but conceptually derives the INS error equations the same.

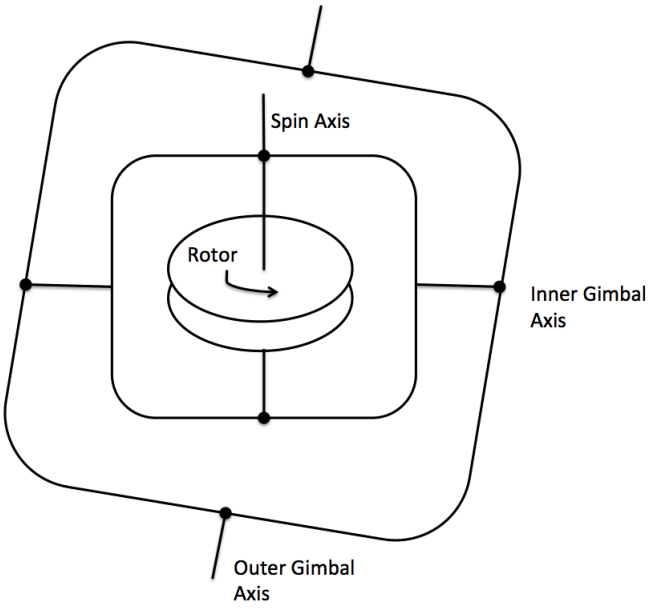

Figure 7. Two-Axis Gyroscope Schematic Diagram

Gyroscope errors come in the form of drift of the spin axis which occurs over time. Hence long navigation scenarios will experience increased gyro drift and require correction.

Strapdown Inertial Navigation.

Strapdown Inertial Navigation refers to inertial systems rigidly attached to the body of the vehicle as compared to a space stabilized system mechanically isolating the INS from body motion via gimbals. Drivers for strapdown system use mainly include size, weight, and cost. The complexity of space stabilized systems are directly related to the size and weight of the system as well as an increase in cost. As mentioned, mechanization is the process of resolving the navigation state information in the navigation frame of reference. Information about the navigation frame of reference

and how it changes over time must be known. For example, the Earths rotation must be taken into account when mechanizing from the body frame to the navigation frame.

INS Error Sources.

The INS inertial instrument cluster made up accelerometers and gyroscopes are susceptible to errors which can be calculated and modeled to enhance performance of the INS navigation solution. Errors will be presented with respect to each sensor, a section for accelerometers and a section for gyroscopes. Although some of the error sources may be modeled similarly, there is a distinct difference in magnitude for the errors in the accelerometers and gyroscopes.

Accelerometer Errors.

Accelerometer error sources covered in this section, specifically apply to the strap-down INS models as there are many different types of accelerometers which have specific errors of their own [21] [23].

- **Bias** - An error source displacing the measurement with a fixed value or slow varying additive error. Bias errors can be determine with inspection of the output with zero acceleration input on the sensitive axis.
- **Scale Factor** - Errors in the conversion from output signal measurements to input acceleration by a scalar quantity. Where the scale factor must be applied to the output signal measurement to determine the input acceleration of the body.
- **Sensor Misalignment** - Sensor misalignment encompasses the manufacturing and installation of the accelerometer sensors. The assumption is the sensors are

all mounted perfectly orthogonal which is physically not practical, leading to sensitive axis measurement errors.

- **Vibration** - External motion vibrations can cause an additional bias error correlated with the sensor vibration environment.

- **Measurement Noise** - Originating from the components used in manufacturing of the sensor, measurement noise encompasses electrical noise, thermal noise, and any other device level noise sources associated with defining the noise level under which a signal cannot be detected.

- **Gravity Model** - Accelerometers measure specific force containing the local gravity component, which must be subtracted out to obtain the acceleration of the body. Local gravity models are calculated based on position. Position is calculated via integration of accelerometer outputs which has error components. Using a position solution corrupted with errors to subtract the acceleration due to gravity from the accelerometer output is the source of the gravity model error.

Gyroscope Errors.

Gyroscope error sources covered in this section limit the accuracy of the Gyroscope's measurement of angular rate. Similar to the accelerometer error sources, techniques for modeling some of the error sources does exist [21] [23].

- **Fixed Bias (g-independent)** - An error source observed at the sensor output when no input angular rotation. This bias is typically a random constant bias or contains slow varying additive error.

- **Acceleration Dependent Bias (g-dependent)** - Proportional to the acceleration force acting on the sensor which impacts not only the sensitive axis of

the sensor but orthogonal axes as well. Orthogonal axes are impacted because of the mass unbalance caused by the acceleration force.

- **Anisoelastic Bias** - Errors associated with acceleration forces present along orthogonal pairs of axes with respect to the sensative axis.

- **Scale Factor** - Errors in the conversion from output signal measurements to input angular rates by way of a scale factor or proportional quantity. The input angular rate is the desired measurement quantity.

- **Sensor Misalignment** - Sensor misalignment refers to the mechanincal manufacturing and installation of the gyroscopes. It is assumed the gyroscopes are mounted in an orthogonal orientation which in physical implementation is not true leading to sensitive axis measurement errors.

- **Measurement Noise** - Originating from the components used in manufacturing of the sensor, measurement noise encompasses electrical noise, thermal noise, and any other noise sources associated with defining the noise level under which a signal cannot be detected.

INS Error Equations.

The dominate INS error sources, described in Section 2.4, drive the direct-state dynamics model at frequencies dependent on relative motion [3]. Therefore, an error model can be applied, encapsulating the INS error which removes the high frequency components of direct-state modeling. The INS error equations are developed to model the errors in Position Velocity Attitude (PVA).

Attitude errors are characterized as the angular error seen in each axis of the navigation frame. The attitude error equation yields a differential equation expressing the change in attitude errors over time [21]. Equation (11) shows the attitude

error dependency on the gyroscope biases $\delta\omega_{ib}^{(b)}$, and the movement of the navigation reference frame in inertial space.

$$\delta\dot{\boldsymbol{\psi}} \approx -\omega_{in}^{(n)} \times \boldsymbol{\psi} + \delta\omega_{in}^{(n)} - \mathbf{C}_b^n \delta\omega_{ib}^{(b)} \tag{11}$$

Velocity error equation dynamics are expressed as Equation (12). Where the Coriolis effect comes into play due to movement in a rotating frame, Earth. Error in the gravity model, $\delta\mathbf{g}$ accounts for the use of the calculated position for the gravity model. Errors in the accelerometer biases, $\delta\mathbf{f}^{(b)}$ are rotated from the body frame to the navigation frame using $\mathbf{C}_b^n$. The skew symmetric form of the forces observed by the accelerometers is $[\mathbf{f}^{(n)}\times]$ which is multiplied by the error in angles $\boldsymbol{\psi}$.

$$\begin{aligned} \delta\dot{\mathbf{v}}^{(n)} = \; & [\mathbf{f}^{(n)}\times]\boldsymbol{\psi} + \mathbf{C}_b^n \delta\mathbf{f}^{(b)} - (2\omega_{ie}^{(n)} + \omega_{en}^{(n)}) \times \delta\mathbf{v} \\ & - (2\delta\omega_{ie}^{(n)} + \delta\omega_{en}^{(n)}) \times \mathbf{v} - \delta\mathbf{g} \end{aligned} \tag{12}$$

The rate of change in position error $\delta\dot{\mathbf{p}}^{(n)}$ is defined as the error in velocity $\delta\mathbf{v}^{(n)}$

$$\delta\dot{\mathbf{p}}^{(n)} = \delta\mathbf{v}^{(n)} \tag{13}$$

Use of the full INS error model can bring about numerical issues and induce more error into the system due to modeling error. Hence, simplification of the INS error model becomes advantageous and has been done while performing research and in industry [17][15][18][22][13].

2.5 Driftmeter

Dating back to World War II bomb targeting, navigators on aircraft like the B-17 and B-24 operated a navigation device known as the driftmeter. At the time, the driftmeter was a measurement of wind drift that allowed the pilot to adjust

trajectories to remain on course while also allowing the navigator to calculate the ground speed for dead reckoning navigation. The use of a drift meter, also known as a drift indicator or drift sight was the only navigation information tool outside of radar ranges from beacons, which were not available in hostile environments. Navigators would sit in the glazed nose of the aircraft and use an to optical sighting device to track arbitrary ground features whenever necessary, like in Figure 8.

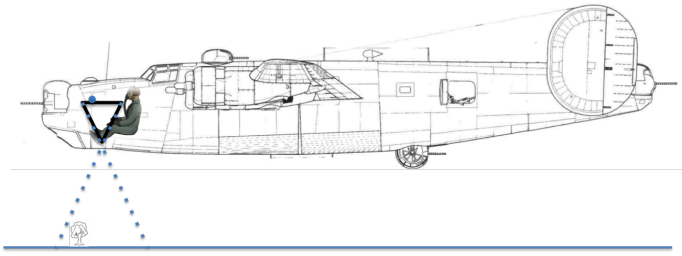

Figure 8. Navigator Locating Ground Feaures with Driftmeter

Many models of the driftmeter were designed and installed for operations on the B-17 and B-24. Figure 9 shows a typical driftmeter. Where the major components are the eyepiece the navigator would look through, the line of sight handle for ground feature tracking along the longitudinal reticle lines, and reading of the drift scale indicating the drift angle.

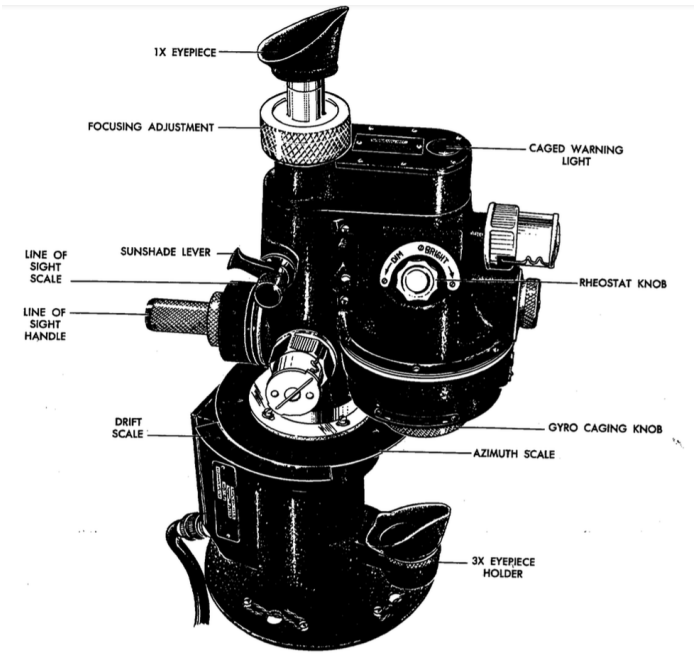

Figure 9. Typical Driftmeter [4]

The driftmeter was made up of a telescoping optical sight attached to a compass scale. On the reticle of the eyepiece, multiple grid lines were etched to aid the navigator in capturing driftmeter measurements. Two or three speed lines were horizontally spaced a known distance. The speed lines along with a timing device were used for speed measurements, providing a ground speed measurement. Tracking a stationary ground feature along the longitudinal grid lines yielded the drift angle due to wind as the navigator rotated the optical sight and observed the compass scale. For example, the aircraft flying a true heading of 100° and the navigator tracks a feature by turning the sighting device to the left 20° indicating the aircraft is drifting 20° to the left with a ground track of 80°. Figure 10 is a visualization of what the navigator would see looking through the eyepiece. By convention, the angle δ is the drift angle rather than the correction angle[4].

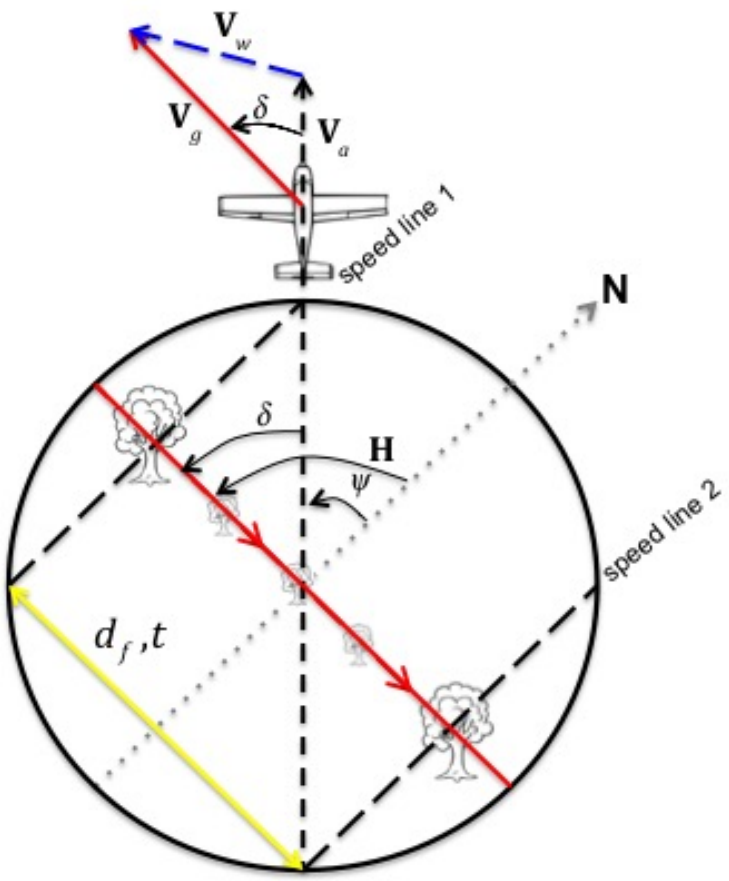

Figure 10. Wind Drift Concept

2.6 Modeling

Based off deterministic modeling techniques, stochastic modeling incorporates a noise component to linear systems in an effort to compensate for deterministic model short comings. Deterministic modeling does not account for certain noise sources that can be observed in the real world, which is where stochastic modeling fills the void. Stochastic models account for mathematical system model imperfections, uncontrollable disturbances impacting the system, and sensor data imperfections [14]. A brief background of deterministic modeling will be presented followed by stochastic modeling which will highlight the additional fidelity associated with stochastic modeling.

Deterministic Modeling.

Deterministic system modeling provides the basis for mathematically capturing the physical aspects of a system. Basic time-domain models of dynamic systems are done in the state space form. The general linear state space equations are shown in Equation (14) in a time invariant application but time varying is also acceptable. In Equation (14), $\mathbf{A}$ is the mathematical dynamics model of the system, $\mathbf{x}(t)$ is the state vector, $\mathbf{\Gamma}$ is the input matrix, and $\mathbf{u}(t)$ is the input vector. The output of the system $\mathbf{z}(t)$ is formed from mapping and scaling the states by way of the obersvation matrix $\mathbf{H}$. Output mapping of system inputs are handled by the $\mathbf{D}$ matrix which is typically zero due to disturbances attributing for most inputs.

$$\begin{aligned} \dot{\mathbf{x}}(t) &= \mathbf{A}\mathbf{x}(t) + \mathbf{\Gamma}\mathbf{u}(t) \\ \mathbf{z}(t) &= \mathbf{H}\mathbf{x}(t) + \mathbf{D}\mathbf{u}(t) \end{aligned} \tag{14}$$

For a linear system modeled derministically, there exists a deterministic solution to Equation (14) which is defined as Equation (15).

$$\mathbf{x}(t) = e^{\mathbf{A}(t-t_0)}\mathbf{x}(t_0) + \int_{t_0}^{t} e^{-\mathbf{A}(t-\tau)}\mathbf{\Gamma}\mathbf{u}(\tau)d\tau \tag{15}$$

Derivation of the state transition matrix $\mathbf{\Phi}$ is achieved through an exponential function of the dynamics matrix in respect to the time step $\Delta t = t - t_0$. The state transition matrix is used to propagate the state vector forward in time based on the dynamics model. State relationships in the time domain are captured in the $\mathbf{\Phi}$ matrix which will be used later to explain obersvability and correlation.

$$e^{\mathbf{A}(t-t_0)} = \mathbf{\Phi}(t - t_0) \tag{16}$$

Observability of a system is defined as the ability to calculate the state based solely

on the system output [11]. For a linear time-invariant system expressed in state space representation, observability can be tested with the row rank of the observability matrix. The output matrix **H** provides a mapping of the states to the output while the dynamics matrix **A** captures the states inter-relationships. Equation (17) forms the observability matrix which test for system observability.

$$\boldsymbol{O}(\mathbf{H}, \mathbf{A}) = \begin{bmatrix} \mathbf{H} \\ \mathbf{HA} \\ \mathbf{HA}^2 \\ \vdots \\ \mathbf{HA}^{n-1} \end{bmatrix} \tag{17}$$

For a system to be completely observable, the row rank of the observability matrix must equal the number of states n. Equation (18) shows the requirements for a fully observable linear time-invariant system.

$$rank\ \boldsymbol{O} = n \tag{18}$$

Deterministic system observability from a theoretic control approach has been investigated by many research efforts, but [1] provides a full analysis of the observability concerns with INS navigation. The observability connection between deterministic system modeling and stochastic system modeling will be explained further in Chapter III.

Stochastic Modeling.

Referring to the beginning of this section (Section 2.6), stochastic modeling increases the fidelity of a model by specifically introducing components accounting for model imperfections, uncontrollable disturbances, and sensor data imperfections. It

is important to first define a stochastic process, which is a real valued function $\mathbf{a}(t, s)$ where t is a time set and s is a set of the sample space which outputs a random variable [14].

The linear system stochastic model addressing the deterministic model gaps is Equation (19). Similar to the deterministic model, the system shown is time invariant, but the framework to model a time variant system exists. Adding to the deterministic model, $\mathbf{G}$ is the noise input matrix which maps the noise realization vector $\mathbf{w}(t)$ to the states, and $\mathbf{v}(t)$ which is the measurement noise vector. Adapting the system to account for any dynamics modeling error is accomplished by $\mathbf{w}(t)$, while $\mathbf{v}(t)$ models real world sensor errors in an attempt to generate more realistic sensor measurements.

$$\begin{aligned} \dot{\mathbf{x}}(t) &= \mathbf{A}\mathbf{x}(t) + \mathbf{\Gamma}\mathbf{u}(t) + \mathbf{G}\mathbf{w}(t) \\ \mathbf{z}(t) &= \mathbf{H}\mathbf{x}(t) + \mathbf{v}(t) \end{aligned} \tag{19}$$

Noise sources, are zero mean, white, Gaussian processes. The noise sources are defined by a process strength or covariance matrix. Process strength $\mathbf{Q}$ is used to define the necessary statistical covariance of the input noise while similarly, $\mathbf{R}$ is used to define the strength of the measurement noise covariance.

$$E\{\mathbf{w}(t) \cdot \mathbf{w}^T(t+\tau)\} = \mathbf{Q}(t) \cdot \delta(\tau) \tag{20}$$

$$E\{\mathbf{v}(t) \cdot \mathbf{v}^T(t+\tau)\} = \mathbf{R}(t) \cdot \delta(\tau) \tag{21}$$

In stochastic modeling, the states composing the state vector $\mathbf{x}(t)$ have an associated covariance. The covariance defines the uncertainty with the state. An understanding of uncertainty is critical in navigation. Where position, velocity, or attitude information may be available, but is not useful without an understanding of

the uncertainty of the available information. The covariance matrix $\mathbf{P}_k$ contains the independent covariances of each state as well as the cross-covariance which quantifies the correlation between states. For example, take a state vector in Equation (22) comprised of random variables ($X, Y, ...etc.$) and a covariance matrix Equation (23).

$$\mathbf{x}(t) = \begin{bmatrix} X \\ Y \\ \vdots \\ n \end{bmatrix}_{1\times n} \tag{22}$$

$$\mathbf{P}_k = \begin{bmatrix} \sigma_{XX}^2 & \sigma_{XY}^2 & \cdots & \sigma_{Xn}^2 \\ \sigma_{YX}^2 & \sigma_{YY}^2 & & \sigma_{Yn}^2 \\ \vdots & & \ddots & \vdots \\ \sigma_{nX}^2 & \sigma_{nY}^2 & \cdots & \sigma_{nn}^2 \end{bmatrix} \tag{23}$$

Independent covariance values for a random variable are located on the diagonal in the $\mathbf{P}_k$ matrix, representing the uncertainty of the random variable. The cross-terms in $\mathbf{P}_k$ are the cross-covariance between two separate random variables. Cross-covariance quantifies a correlated relationship between random variables. Where correlation is defined as a measure of the relational strength between two separate random variables.

From probability theory and statistics, the state vector variables are modeled as random variables. The covariance of random variables can be established using the expected value operator. Equation (24) shows the variance relationship in probability and statistics used to populate the covariance matrix.

$$\sigma_{XY}^2 = E[(X - \mu_X)(Y - \mu_Y)] \tag{24}$$

Where μ is the mean of the random variable, and X or Y is the random variable.

First Order Gauss Markov Process.

A First Order Gaussian Markov (FOGM) process [14] takes on multiple statistical properties which are used to model bias behaviors of accelerometers and gyroscopes. First, a Markov Process is characterized by the Markov Property defined as memoryless. Equation (25) mathematically expresses the Markov property of recursion.

$$f(x_k \mid x_{k-1} \ ... \ x_N) = f(x_k \mid x_{k-1}) \qquad \forall k \in \mathbb{R}, k-1, ..., N < k \in \mathbb{R} \tag{25}$$

A Gaussian Process can be characterized simply with mean and variance of the process. The Normal or Gaussian Probability Distribution Function (PDF) and Cumulative Distribution Function (CDF) are well known to be Equation (26).

$$\begin{aligned} f(x, \mu, \sigma) &= \frac{1}{\sigma\sqrt{2\pi}} e^{-\frac{(x-\mu)^2}{2\sigma^2}} \\ F(x) &= \frac{1}{\sqrt{2\pi}} \int_{-\infty}^{x} e^{\frac{-t^2}{2}} dt \end{aligned} \tag{26}$$

Measurement Models.

Measurement models are used to take physical sensors capable of measuring physical space to the simulation space by way of mathematical characterization. The process by which a sensor is modeled mathematically is extensively documented in [8] and [14] while also being verified in community research.

Specifically in the research presented, two measurement models will be introduced. A bearing or angle measurement model, and a linear single state model. The angle measurement model serves as a good background for the measurement model applied in Chapter III. The linear single state model is used in Chapter III to model a barometer altitude aiding sensor.

Angle Measurement Model.

A bearing measurement is defined as the angle between two points within a coordinate frame of reference. Information about the direction vector connecting the points exists with the absence of range. With knowledge of the position of both points, trigonometric functions enable the calculation of the angle between the points. To illustrate the information necessary for the measurement model and the output solution, an example is presented. Take an aircraft flying in 2-D position space receiving angle measurements to a beacon, referenced as a target (T) located at $\binom{x_T}{y_T}$.

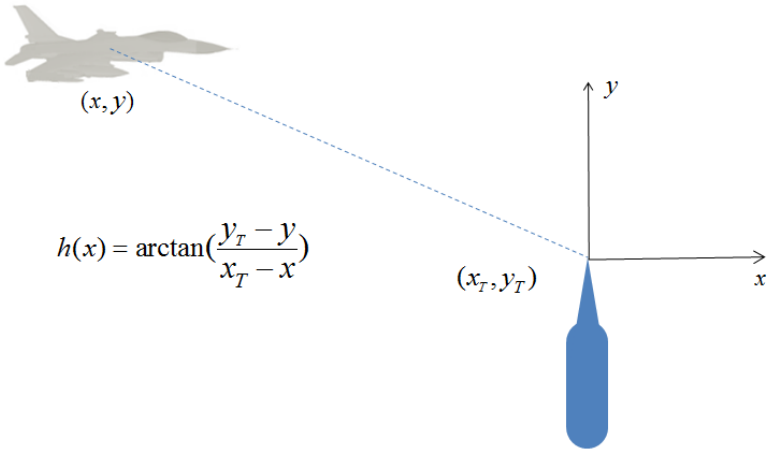

Figure 11. General Angle Measurement Model

Equation (27) shows the angle measurement equation which is non-linear and must be accounted for when used directly in Kalman filtering.

$$h(\hat{\mathbf{x}})_{\text{angle}} = \arctan\left(\frac{y_T - y}{x_T - x}\right) \tag{27}$$

Therefore, a Jacobian approximation is used when implementing an Extended Kalman Filter (EKF) which handles the non-liniearities in the dynamics and measurement model. However, there is still a degree of linearization error associated with linearizing the measurement model [14]. The Jacobian approximation for the angle

measurement model presented in Equation (27) is shown in Equation (28).

$$\begin{aligned} \frac{\partial h(\hat{\mathbf{x}})_{angle}}{\partial x} &= \frac{y_T - y}{(x_T - x)^2 + (y_T - y)^2} \\ \frac{\partial h(\hat{\mathbf{x}})_{angle}}{\partial y} &= \frac{x - x_T}{(x_T - x)^2 + (y_T - y)^2} \end{aligned} \tag{28}$$

Where the partial derivative of the measurement equation is taken with respect to the state. Other linearizion techniques are possible when manipulating the information captured from an angular measurement and will be presented in Chapter III.

Geometry Based Bearing Measurements.

Pure bearing measurements provide radial information while the range is unobservable. If the range can be constrained with known information, then the bearing measurement becomes a much more information rich aiding source. In the case where an aircraft is flying and taking bearing measurements to features located on the Earth's surface, knowledge of elevation data or even use of a barometric altimeter could be used to constrain the elevation of the ground feature.

The E/O system provides a measurement of the ground feature in the inverted image plane d_l while the focal distance of the camera is known f. Altitude of the aircraft h is typically known well with a barometric aiding source and the distance from the aircraft's ground projection to the ground feature is d. Invoking a similar triangle relationship, Equation (29) captures the proportional relationship between what the E/O system measures and the aircraft's location in (x, z).

$$\frac{d_l}{f} = \frac{d}{h} \tag{29}$$

Derived in a 3-dimensional case, the aircraft's true position and the true position of the ground feature maintain a relationship through geometry [18]. Equation (30) shows the geometry relationship between the true aircraft position (x, y, z),

the true ground feature position (x_p, y_p, z_p), and the measurements from the E/O system (x_f, y_f). The focal length of the E/O system is f, $\mathbf{C}_b^n$ is the DCM transformation from the body frame to the navigation frame.

$$\begin{pmatrix} x_p \\ y_p \\ z_p \end{pmatrix} = \begin{pmatrix} x \\ y \\ z \end{pmatrix} + \frac{|R_{LOS}|}{\sqrt{x_f^2 + y_f^2 + f^2}} \mathbf{C}_b^n \begin{pmatrix} x_f \\ y_f \\ -f \end{pmatrix} \tag{30}$$

The similar triangle relationship can be explicitly observed in the $\frac{|R_{LOS}|}{\sqrt{x_f^2+y_f^2+f^2}}$ term where the measurement from the E/O system is used to scale the R_{LOS} from the aircraft to the ground feature. Independently separating Equation (30) yields three individual measurement equations:

$$x_p - x = \frac{|R_{LOS}|}{\sqrt{x_f^2 + x_f^2 + f^2}} \begin{pmatrix} 1 & 0 & 0 \end{pmatrix} \mathbf{C}_b^n \begin{pmatrix} x_f \\ y_f \\ -f \end{pmatrix} \tag{31}$$

$$y_p - y = \frac{|R_{LOS}|}{\sqrt{x_f^2 + x_f^2 + f^2}} \begin{pmatrix} 0 & 1 & 0 \end{pmatrix} \mathbf{C}_b^n \begin{pmatrix} x_f \\ y_f \\ -f \end{pmatrix} \tag{32}$$

$$z_p - z = \frac{|R_{LOS}|}{\sqrt{x_f^2 + x_f^2 + f^2}} \begin{pmatrix} 0 & 0 & 1 \end{pmatrix} \mathbf{C}_b^n \begin{pmatrix} x_f \\ y_f \\ -f \end{pmatrix} \tag{33}$$

Assuming knowledge of ground feature elevation information z_p, manipulation through substitution can constrain the R_{LOS} which can be substituted into the remaining two equations for the x and y axes. After manipulation of Equation (33), Equation (34) is the scaled R_{LOS} which can be substituted into Equations (31) and (32).

$$\frac{|R_{LOS}|}{\sqrt{x_f^2 + y_f^2 + f^2}} = \frac{z_p - z}{\begin{pmatrix} 0 & 0 & 1 \end{pmatrix} \mathbf{C}_b^n \begin{pmatrix} x_f \\ y_f \\ -f \end{pmatrix}} \tag{34}$$

Referencing back to Equations (31) and (32), Equation (34) can be substituted in yielding Equation (35) which is incorporating the knowledge of ground feature elevation data.

$$\begin{pmatrix} x_p \\ y_p \end{pmatrix} = \begin{pmatrix} x \\ y \end{pmatrix} + \frac{z_p - z}{\begin{pmatrix} 0 & 0 & 1 \end{pmatrix} \mathbf{C}_b^n \begin{pmatrix} x_f \\ y_f \\ -f \end{pmatrix}} \begin{bmatrix} 1 & 0 & 0 \\ 0 & 1 & 0 \end{bmatrix} \mathbf{C}_b^n \begin{pmatrix} x_f \\ y_f \\ -f \end{pmatrix} \tag{35}$$

Linear Single State Measurement Model.

Use of a simple linear state model is applicable when modeling relatively linear measurement sensors containing error sources that can be characterized with biases or Gaussian white noise. Recall Equation (19) where the measurement model is linearly formed by mapping the state vector to measurement space plus white Gaussian noise. In the simple 2-D space position model used in Section 2.6, a barometric sensor in the 2-D case would be able to measure the Y channel. The measurement model for the two state system example would be

$$\mathbf{z}(t) = y + v_k \tag{36}$$

where the observation matrix would map the y state to measurement space and add white Gaussian noise account for sensor errors. This linear measurement model is useful in applications where deriving a linear model is possible.

2.7 Kalman Filtering

Kalman filtering serves as a bedrock of navigation estimation Bayesian Filtering. A Kalman filter is an optimal recursive data processing algorithm, specifically the optimal Minimum Mean Squared Estimator (MMSE)[14]. Implementing a KF begins

with with initial conditions, dynamics model, measurement model, and characterization of noise sources. Two implementations of a KF with respect to inertial navigation are widely used, direct state (*total state space*), and indirect state (*error state space*).

Direct State Kalman Filtering.

Direct state Kalman Filters estimate the actual states such as vehicle position, velocity, and attitude. The drawbacks of direct state Kalman filtering are the high sampling rates required due to high frequency dynamics. Therefore, direct state KFs are not typically used in real-time navigation applications. Direct mechanization is typically restricted to alignment, calibrations, and bias determination in a testing environment [14].

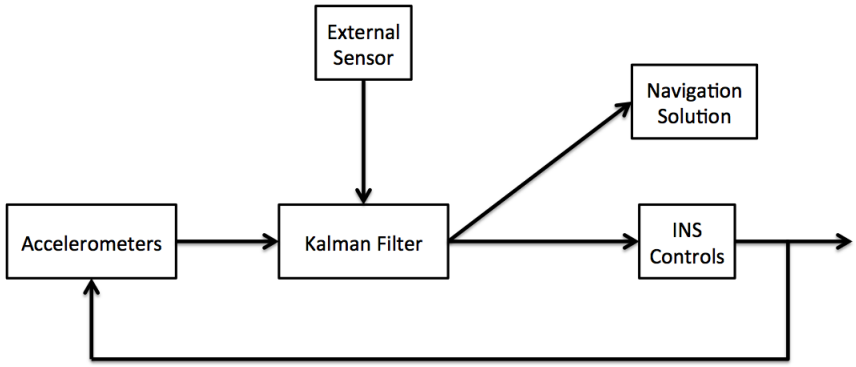

Figure 12. Direct State Inertial Navigation Kalman Filter Block Diagram

Indirect State Kalman Filtering.

Indirect state Kalman Filters estimate the errors in a particular information source compared to an external source. In the case of inertial navigation research, the indirect state Kalman filter will estimate the error in the INS using the difference between the INS output and the external sensor. In the case of vision aided navigation, the external sensor is an optical measurement device providing information to the Kalman

filter via images. Tracking of features over time and their movement in the image plane, with the assumption the ground features are stationary, generates useful information the Kalman filter can use to update the state vector. High frequency dynamics are captured in the INS sampling due to the robustness of the error model while the system error propagation is dominated by the low frequency error propagation model.

Figure 13 shows an indirect state Kalman filter with a feedforward implementation. The feedforward is executed by taking the output of the Kalman filter error estimates and subtracting the error estimate from the INS solution. In this system model, the INS is completely running free without input from outside correction sources. Strictly the output of the INS is corrected rather than a resetting or direct correction to the inertial system which has pros and cons. The benefit lies in the self contained nature of the INS which will still be able to operate during measurement outages and filter unreliabilities. However, if measurements from the external source become unavailable, the navigation solution will revert to the free running INS errors as if no aiding existed from the external source.

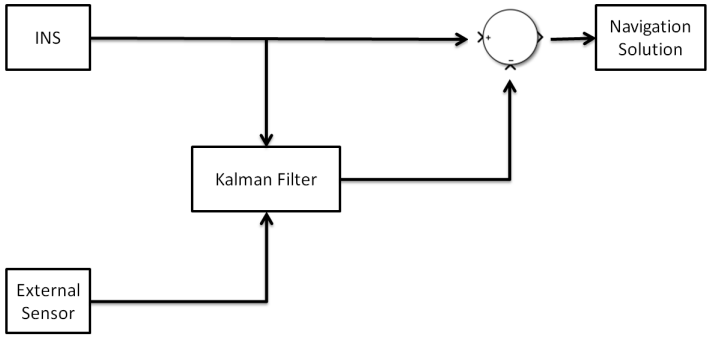

Figure 13. Indirect State Feedforward Inertial Navigation Kalman Filter Block Diagram

An indirect state feedback filter is shown in Figure 14. Compared to the feedforward indirect state Kalman filter, the feedback filter provides direct correction to the inertial system. This method of filtering maximizes the use of the error estimation

but also presents system level concerns. As the inertial system has become dependent on the Kalman filter and the measurements from the external sensor. Erroneous measurements from the external sensor have the potential to corrupt the INS without the ability to revert back to the self contained INS like the feedforward implementation.

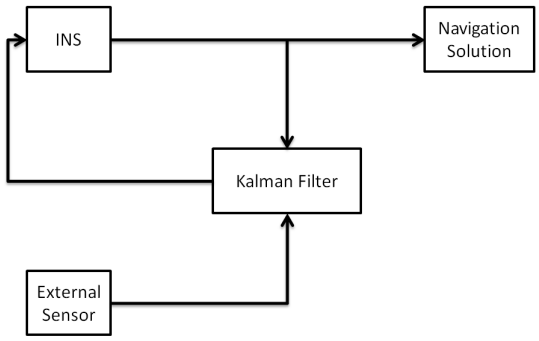

Figure 14. Indirect State Feedback Inertial Navigation Kalman Filter Block Diagram

Kalman Filter Equations.

The Kalman filter, introduced by Rudlof E. Kálmán in a paper titled "A New Approach to Linear Filtering and Prediction Problems" initiated the connection between the state estimate conditioned on previous measurements. A state-space system formulation is used with a dynamics model, control inputs, and measurement model. As a recursive algorithm, the Kalman filter uses information from the previous time iteration to calculate the current time iteration state vector and covariance matrix. Optimal in the MMSE sense, an estimate of the state vector conditioned on all measurements available is realized; shown in Equation (37).

$$\hat{\mathbf{x}}_k = E[\mathbf{x}_k \mid \mathbf{Z}_k] \tag{37}$$

Operation of the Kalman filter is in discrete time, but at each discrete time step there exists two instances of the KF estimate $\hat{\mathbf{x}}_k$ and the covariance matrix $\mathbf{P}_k$ that approach the discrete time step from opposite sides. The two instances of the estimate

and covariance stem from the presence of an update at time k. An estimate with an update $\hat{\mathbf{x}}_k^+$ will be moved forward to the next time step through propagation yielding $\hat{\mathbf{x}}_{k+1}^-$. Upon update, at the same time step, the KF estimate becomes $\hat{\mathbf{x}}_{k+1}^+$.

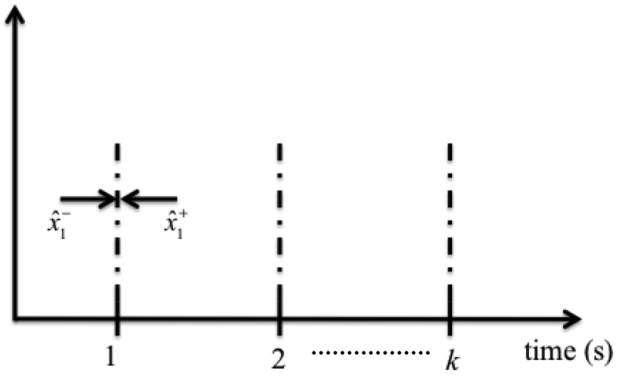

Figure 15. Kalman Filter Time Defined

The Kalman filter can be implemented as an online estimation algorithm due to the recursive nature of the bayesian estimation filter. Figure 16 shows the recursive nature of the Kalman filter and the discrete-time estimation process.

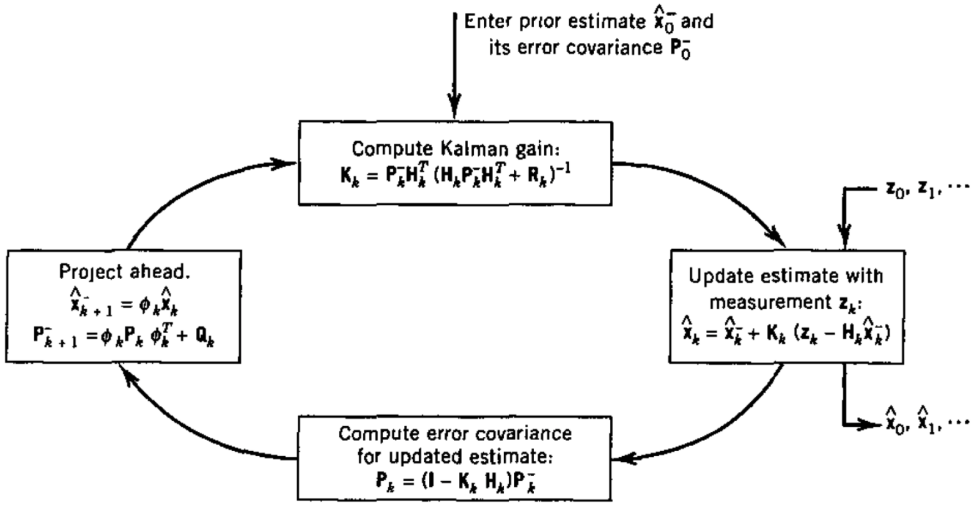

Figure 5.8 Kalman filter loop.

Figure 16. Indirect State Feedback Inertial Navigation Kalman Filter Block Diagram[14]

Propagate.

Time propagation in the Kalman filter projects the estimate of the states based on the dynamics model defined forward in time. Where the time step is defined by the $(t - t_0)$ used to generate the discrete time state transition matrix $\mathbf{\Phi}_d$. In vision aided-INS navigation research, the additive noise sources are the drift and bias associated with the sensors measuring specific force and angular rate. Propagation of the state vector is accomplished with multiplication of the state transition matrix, calculated from the dynamics model, with the previous state vector estimate. The covariance matrix is also propagated forward in time with the state transition matrix along with additive discrete input noise. Kalman filter propagation equaitons are shown in Equation (38). Where $\hat{\mathbf{x}}_k^-$ is the state estimate before update, denoted with the superscript "-" accent.

$$\begin{aligned} \hat{\mathbf{x}}_{k+1}^- &= \mathbf{\Phi}_d \hat{\mathbf{x}}_k^+ \\ \mathbf{P}_{k+1}^- &= \mathbf{\Phi}_d \mathbf{P}_k^+ \mathbf{\Phi}_d^T + \mathbf{Q}_d \end{aligned} \tag{38}$$

Observation Matrix.

The observation matrix $\mathbf{H}_{k+1}$, similar to the deterministic system output matrix, maps the states to measurement space. Modeling the KF measurement $\bar{\mathbf{z}}_{k+1}$, the observation matrix is multiplied by the states and the measurement noise $\mathbf{v}_{k+1}$ is added to the resultant. Equation (39) shows the modeling of KF measurements where $\mathbf{H}_{k+1}$ is the measurement model, or matrix for a linear case, and $\mathbf{v}_{k+1}$ is the noise associated with the external sensor providing update information to the Kalman filter. Camera noise sources will be discussed further in the digital imaging Section 2.8.

$$\bar{\mathbf{z}}_{k+1} = \mathbf{H}_{k+1} \hat{\mathbf{x}}_{k+1} + \mathbf{v}_{k+1} \tag{39}$$

Update.

State estimate updating in a Kalman filter requires a measurement $\bar{\mathbf{z}}_{k+1}$ to be available for the current time step, referencing Equation (37). If a measurement is not available, no update step is executed and the Kalman filter will continue propagating the estimate to the next time step. When a measurement is available, information from an external sensor will be used to update the current estimates.

$$\begin{aligned} \hat{\mathbf{x}}_{k+1}^{+} &= \hat{\mathbf{x}}_{k+1}^{-} + \mathbf{K}_{k+1}(\bar{\mathbf{z}}_{k+1} - \mathbf{H}_{k+1}\hat{\mathbf{x}}_{k+1}^{-}) \\ \mathbf{P}_{k+1}^{+} &= (\mathbf{I} - \mathbf{K}_{k+1}\mathbf{H}_{k+1})\mathbf{P}_{k+1}^{-} \end{aligned} \tag{40}$$

Minimization of the mean-squared estimation error is specifically accomplished with the Kalman gain term $\mathbf{K}_{k+1}$ [8]. The Kalman gain is a weighting term that scales the residual $\bar{\mathbf{z}}_{k+1} - \mathbf{H}_{k+1}\mathbf{x}_{k+1}^{-}$ based on the covariance matrix, the measurement model, and the measurement noise. Filter performance can be specifically tracked with the residual.

$$\mathbf{K}_{k+1} = \mathbf{P}_{k+1}^{-}\mathbf{H}_{k+1}^{T}(\mathbf{H}_{k+1}\mathbf{P}_{k+1}^{-}\mathbf{H}_{k+1}^{T} + \mathbf{R})^{-1} \tag{41}$$

Residual.

An understanding of filter performance is a vital metric when optimizing a filter for a specific application. Performance of the filter is accomplished with comparing the filter's estimate of the measurement versus the measurements provided by the external source. The comparison of the filter estimate and the external source measurement is know as the residual. Equation (42) shows the measurement residual and residual covariance which are a performance metrics showing how the filter can estimate the measurements from the external source.

$$\begin{aligned} \mathbf{r}_{k+1} &= \bar{\mathbf{z}}_{k+1} - \mathbf{H}_{k+1}\hat{\mathbf{x}}_{k+1}^{-} \\ \mathbf{S}_{k+1} &= \mathbf{H}_{k+1}\mathbf{P}_{k+1}\mathbf{H}_{k+1}^{T} + \mathbf{R} \end{aligned} \tag{42}$$

2.8 Digital Imaging

A digital imaging system, specifically a camera, takes in light from a scene through optics which are detected, amplified, and digitized into a digital output. The use of a digital imaging system for inertial system aiding is done by the E/O system. Camera models, noise sources, and image registration topics relevant to this research will be explained in this section.

Camera Models.

An illustration of an image system model is shown in Figure 17. A scene is created from the reflection of light off objects in the world. The scene is captured as the reflected light enters the optics of the imaging device. Optics change the direction of the light via a convex lens to focus the light to the optical center of the camera and project the inverse scene onto the detector. Variations in thickness and shape of the optics will change the parameters of how the scene is projected onto the detector. When light hits the detector, photons are converted to charges, and transferred by rows in a raster fashion. The voltage signal is then amplified prior to digitization yielding a digital output of the scene observed. Analysis of the digital output from the imaging system enables the feature tracking done in image aided inertial navigation.

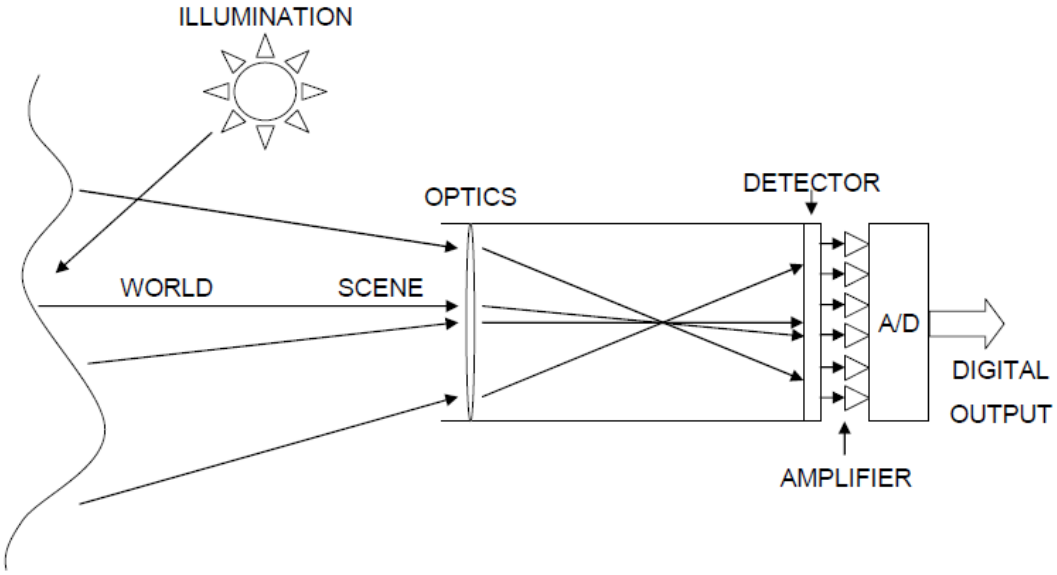

Figure 17. Image System Model[23]

Pinhole Camera Model.

The pinhole camera model in Figure 18 is a theoretical concept assuming the thin lens aperture approaches zero. As the thin lens aperture approaches zero, light from the scene will be focused to pass through the aperture at the exact same intersection point. When the scene is projected onto the image frame in the pinhole model, the scene is actually inverted. Projecting the inversion of the image frame yields a projection of the scene in front of the aperture the length of the focal distance.

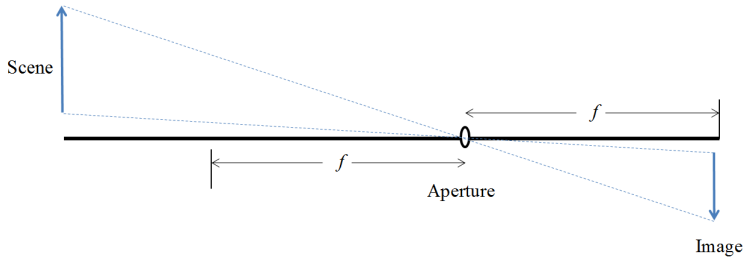

Figure 18. Pinhole Camera Model

Camera Noise Model.

Multiple sources of noise are present in Charge Coupled Device (CCD) camera images, which are used on targeting pods. CCD noise sources include the conversion of optical photons to electrical signal charges and the probabilistic measurement error due to sampling. Noise associated with the external sensor providing update information to the Kalman filter is critical. The associated variance of the measurements brought into the filter must be valid. For example, if the measurements brought into the Kalman filter have an incorrectly associated variance that is smaller than the true value, the Kalman filter will incorrectly trust the measurements when updating the filter estimate.

Image Registration.

Although image registration will not be implemented in this research, computer vision is a vital component to image-aided navigation. Image registration brings about issues like camera calibration, feature-point matching techniques, and computational burdens. Camera calibrations are used to capture the parameters describing the mapping of 3-dimensional scene space to the 2-dimensional image plane space. Theoretical simulations can be performed with the pin hole camera model, but in experimental testing the distortion caused by imperfections in the camera lens must be modeled and accounted for when using feature-point matching for navigation. A closed-form solution to modeling radial distortion [25] was developed by Zhang which has since been extended and improved upon for use in camera calibration toolboxes.

A tutorial on *Visual Odometry*, specifically *Part II: Matching, Robustness, Optimization, and Applications* dives deep into explaining the current applications of Visual Odometry and the techniques used to provide relative position error ranging from 0.1 to 2% [19]. Fundamentally, two approaches exist to track features. One,

identifying features in one image and subsequently tracking those same features' properties throughout future images. Two, independently detecting features in images and matching the features based on similarity characteristics. Frandorfer and Scaramuzza present a review of the main feature-point techniques used in Visual Odometry, including popular blob detectors Scale Invariant Feature Transformation (SIFT), Speeded Up Robust Transformation (SURF), and Center Surround Extremas (CENSURE).

2.9 Related Research

There is no shortage of research on aiding an INS. With the emergence of GPS, the accuracy and precision provided ideal aiding action to an INS for navigation. However, the reliability of GPS in specific operating environments has ignited the research on passive sensors to aid an INS. Specifically, at the Air Force Institute of Technology (AFIT) Autonomy and Navigation Technology (ANT) Center, vision-aided inertial systems are a strong research thrust. This section does not by any means represent an exhaustive representation of the communities research but does highlight the research used to motivate and guide the work presented.

Inertial Navigation System Aiding Using Vision.

James Quarmyne investigated a scripted navigation scenario problem similar to the research presented, where two ground features were placed in the field of view of the optical sensor used to aid the INS. The Simultaneous Localization and Mapping (SLAM) approach was used to constrain the growth of the INS errors over time. Augmenting the state vector with the geolocated position of the ground features, along with the covariances, for the duration of the flight significantly reduces the INS error growth [17].

Fusion of Low-Cost Imaging and Inertial Sensors for Navigation.

Mike Veth presented a fusion of low cost imaging and inertial sensor integration for navigation. Utilizing a tightly coupled system structure at the measurement level, benefitting from the reliability of the inertial system over short time periods and the duration reliability of the imaging sensor measurements. Monte Carlo analysis was done to simulate the indoor profile where features were randomly generated on walls to formulate expected performance of the integrated system. Experimental testing in the hallways of AFIT showed that using the tightly coupled system along with stochastic feature projection, the navigation solution error was significantly constrained [24].

A Covariance Analysis of Vision-Aided Inertial Navigation: 3-D Case.

Relyea and Pachter investigated the "bootstrapping" method for INS aiding during a cross country flight where previously identified ground features do not reappear in the field of view. The transition from using the known location of ground features for INS updating to using unknown ground features for INS updating is covered. Where the system is augmented with the position estimate and covariance associated with the ground features used for the INS aiding. It was shown that the growth in the errors are still unbounded but the rate of growth was significantly reduced. The volume of position uncertainty was defined for an unaided INS as 0.7071 km^3 which was reduced to 7.4177 $\times 10^{-10}$ with optical tracking aided INS where ground features were successively tracked throughout the flight [18].

INS Aiding Using Passive Bearings-Only Measurements Of An Unknown Stationary Ground Object.

Alec Porter constructed three main scenarios where bearings-only measurements were used to aid a tactical-grade INS with and without prior information, and the

impact of bearings-only measurements at varying altitudes. The altitude dependency was evident as the true bearing and INS corrupted bearing cannot be assumed equal with the presence of significant altitude error. His analysis showed that without prior knowledge, the positional accuracy of the aircraft is minimally aided. Where the bearing measurements used are more effective with high Signal-to-Noise Ratio (SNR) Line of Sight (LOS) measurements in a low Geometric Dilution of Precision (GDOP) flight scenario with the stationary ground feature.

III. Methodology

The methodology of the conducted research will be presented as a step by step process that was initially equation derived and then validated in simulation. First, an understanding of what World War II navigators were able to provide operating a driftmeter. Also, defining the robustness associated with the INS error model due to maneuvering flight dynamics versus a steady-state flight condition will be evaluated. Then, using current technology to generate "driftmeter" measurements for INS aiding. A wings level, constant airspeed, heading and altitude hold flight is simulated to capture what a contemporary driftmeter brings to the table.

When working with non-dimensional variables and parameters, it is important to calibrate expected performance. The INS error source covered in this research will strictly be the accelerometer and gyroscope biases. As the dominant source of accumulating INS error, it makes sense to begin with with strictly the bias error sources to test performance. Rather than a plug and play approach with known specifications of bias error σ values provided by manufactures, the non-dimensional σ values were simulated. Calibrated INS bias standard deviations were used to propagate the simulated navigation state INS errors that would be experienced during a flight. Based on the INS calculated PVA, determined from both the flight trajectory and navigation state error realization, simulated bearing angle measurements to a stationary ground feature are calculated. Initialization of the Kalman filter is a very important facet of the INS aiding technique presented and will be developed further in the section. At the conclusion of a measurement epoch, the INS is reset by subtracting out the Kalman filter navigation state error estimate, yielding theoretically a more accurate INS calculated PVA solution. The purpose of collecting measurements throughout the epoch and updating at the end is to gauge the strength of INS aiding.

Presentation of the INS aiding methods will be accomplished in two stages. Method

1 will be referred to as Navigator Replication where the functions of the navigator will be directly mechanized and assumptions are made about what the navigator had available. Method 2 is the implementation of the measurement equation derived in Section 3.4 where contemporary technology is used to automate the functions of the navigator and the driftmeter.

3.1 Experiment

The experiment of this vision-aided inertial navigation research lies in the estimation of the error in velocity δv_x of the INS. Tracking a ground feature throughout a measurement epoch with an E/O system provides information about the INS error in velocity. Based on the INS error model dynamics, correlation will be leveraged by the Kalman filter to effectively reduce the INS error growth for the remainder of the flight following a measurement epoch. If possible, estimating a portion of the accelerometer bias, which is a major source of INS error could also positively impact the resulting INS solution following a measurement epoch [12].

3.2 Navigation Scenario

The navigation scenario section of the methodology will serve as a baseline of assumptions and conditions set for the vision-aided inertial navigation research simulations. Although some of the assumptions and simplifications appear to make the work novel, the goal is to determine the strength of INS aiding possible with a vision sensor if a ground feature is tracked manually by a pilot. Implementation and real-world testing is possible with this research as the next logical step to reduce IP update constraints.

Non-Dimensionalization.

Variables have been non-dimensionalized via substitution to eliminate variable units according to Table 1.

Table 1. Navigator Driftmeter Replication Non-Dimensionaliztion

Position	Velocity	Specific Force Error	Angular Rate Error	Time
x $\rightarrow \frac{x}{h}$	$v_x \rightarrow \frac{v_x}{v}$	$\delta f_x^{(b)} \rightarrow \frac{\delta f_x^{(b)}}{g}$	$\delta\omega_x^{(b)} \rightarrow h\frac{\delta\omega_x^{(b)}}{v}$	$t \rightarrow t\frac{v}{h}$
y $\rightarrow \frac{y}{h}$	$v_y \rightarrow \frac{v_y}{v}$	$\delta f_y^{(b)} \rightarrow \frac{\delta f_y^{(b)}}{g}$	$\delta\omega_y^{(b)} \rightarrow h\frac{\delta\omega_y^{(b)}}{v}$	$T \rightarrow T\frac{v}{h}$
z $\rightarrow \frac{z}{h}$	$v_z \rightarrow \frac{v_z}{v}$	$\delta f_z^{(b)} \rightarrow \frac{\delta f_z^{(b)}}{g}$	$\delta\omega_z^{(b)} \rightarrow h\frac{\delta\omega_z^{(b)}}{v}$	$\Delta t = 1$

Constant aircraft flight simulation parameters used to non-dimensionalize variables are listed in Table 2:

Table 2. Steady-State Flight Constants

h	$1000\ m$
g	$10\frac{m}{s^2}$
v	$100\frac{m}{s}$

Non-dimensionalization of all variables and parameters simplify calculations and prevent errors with units. Acceleration due to gravity is taken to be constant and rounded to 10 $\frac{m}{s^2}$. Equation (43) lays out the non-dimensionalization process executed for all variables in Table 1.

$$g \rightarrow \frac{h \cdot g}{v^2} = \frac{1000\,m \cdot 10\frac{m}{s^2}}{(100\frac{m}{s})^2} = \frac{10000\frac{m^2}{s^2}}{10000\frac{m^2}{s^2}} = 1 \tag{43}$$

Flight Conditions.

Replication of the navigator's operation of the driftmeter is done through a simulated 1 hour flight. During the course of the flight, the INS errors will accumulate without an aiding source. Halfway through the flight, 30 minutes, a ground feature will be tracked for the duration of an epoch. The flight is broken up into epochs which are 10 time steps (seconds) long in duration. Therefore, the entire flight consists of 360 epochs. Throughout the duration of the flight, the aircraft will be in autopilot mode: winds level, airspeed, altitude, and heading hold. Theoretical wings level flight conditions indicate no attitude changes in roll and pitch (ϕ, θ). Due to external forces like wind, wings level flight assumes small attitude changes in roll and pitch exist to maintain wings level flight, but are small and cancel out in nature. Airspeed hold describes a constant velocity flight condition where the aircraft is not accelerating or decelerating. Maintaining altitude simplifies the the vertical component of the LOS vector to the tracked ground feature. Heading hold constrains (ψ), maintaining a constant aircraft direction of travel. The scripted steady-state flight dynamics eliminate analysis ambiguities so the aiding action associated with driftmeter measurements can be understood.

Measurement Geometry.

Geometry of the navigation scenario and measurement arrangement is visualized in Figure 19. The projection of the aircraft position is the position of the aircraft on the surface of the Earth. Denoted with the variable P, the tracked stationary ground feature's height is assumed known via elevation data or calculation with the barometric altimeter. The aircraft body frame (x_b, y_b, z_b) is conveniently in the same orientation as the navigation reference frame (x_n, y_n, z_n) which is in an East-North-Up convention. Aircraft direction of travel will be in the East direction, longitudinal

velocity will be the only dynamics induced into the system. The camera frame of the E/O system is rigidly attached to the aircraft and co-located with the body frame of the aircraft.

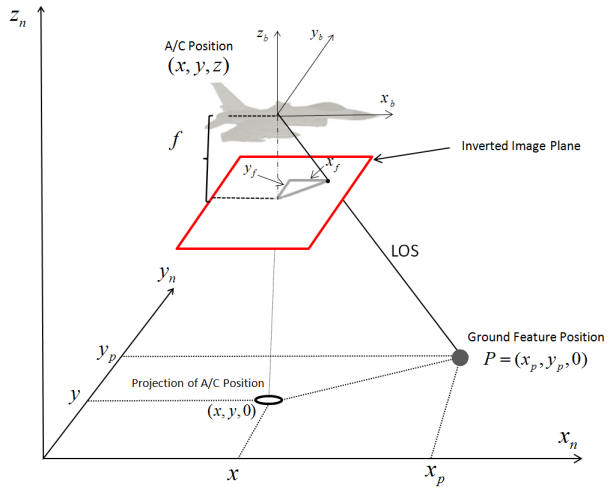

Figure 19. Navigation Geometry of Measurement Arrangement

Longitudinal travel in the x_n axis will cause the stationary ground feature to move through the inverted image plane only in x_f. Where (x_f, y_f) are the pixel location of the ground feature in the inverted image plane. The inverted image plane is non-dimensionalized with the focal distance, f, and is therefore 1 x 1 non-dimensional. With the center of the inverted image plane defined as (0,0), a feature entering the field of view of the E/O system will be at $\binom{x_f}{y_f} = \binom{0.5}{0}$. Where the value of a ground feature entering the E/O system is positive because the image plane is inverted. The measurement equation will be covered in Section 3.4.

INS Error Model - Dynamics.

Error state dynamics are formed based on the INS error equations developed in Section 2.4, with simplifications. The errors propagated forward in the time domain are defined as the true navigation state minus the INS calculated navigation state in Equation (44) where $\mathbf{x}$ is the true PVA navigation state vector and $\mathbf{x}_c$ is the calculated

INS navigation solution corrupted with $\delta\mathbf{x}$ errors.

$$\delta\mathbf{x} = \mathbf{x}_c - \mathbf{x} \tag{44}$$

The navigation state error vector is defined as

$$\delta\mathbf{x} = \begin{bmatrix} \delta\mathbf{p}^{(n)}, & \delta\mathbf{v}^{(n)}, & \delta\boldsymbol{\psi} \end{bmatrix}^T \tag{45}$$

where $\delta\mathbf{p}^{(n)}$ are position errors in the navigation frame, $\delta\mathbf{v}^{(n)}$ are velocity errors in the navigation frame, and $\delta\boldsymbol{\psi}$ is the angular error vector of the ENU navigation frame of reference. Accelerometer and gyroscope biases will be brought into the system as inputs according to

$$\delta\mathbf{u} = \begin{bmatrix} \delta f_x^{(b)}, & \delta f_y^{(b)}, & \delta f_z^{(b)}, & \delta\omega_x^{(b)}, & \delta\omega_y^{(b)}, & \delta\omega_z^{(b)} \end{bmatrix}^T \tag{46}$$

The continuous time state space stochastic model is expressed in a linear arrangement which is driven by the input vector and white Gaussian noise [14]:

$$\dot{\mathbf{x}}(t) = \mathbf{A}\mathbf{x}(t) + \boldsymbol{\Gamma}\mathbf{u}(t) + \mathbf{G}\mathbf{w}(t) \tag{47}$$

The state transition matrix is derived from the continuous time dynamics model of error propagation. Rather than direct state modeling, error state modeling affords the ability to capture the impact of high frequency dynamic maneuvers with low frequency sampling rates. The continuous time model for PVA used in this research will be developed next.

Attitude errors are characterized as the angular error seen in each axis of the navigation frame. The attitude error development from Section 2.4 yielded a differential equation expressing the change in attitude errors over time [21]

$$\delta\dot{\boldsymbol{\psi}} \approx -\omega_{in}^{(n)} \times \boldsymbol{\Psi} + \delta\omega_{in}^{(n)} - \mathbf{C}_b^n \delta\omega_{ib}^{(b)}$$

The flight trajectory defined in Section 3.2 allows simplifications to the attitude error differential equation. The constant velocity flight path along the x_n axis and navigation over a flat and non-rotating Earth eliminates the error in the turn rate of the navigation frame $\delta\omega_{in}^{(n)}$. Therefore, the change in angular error can now be expressed as

$$\delta\dot{\boldsymbol{\psi}} \approx -\mathbf{C}_b^n \delta\omega_{ib}^{(b)} \tag{48}$$

For small Euler angles (ψ, θ, ϕ) and an aligned body to navigation frame, the DCM performing reference frame transoformations from the body frame to the navigation frame is

$$\mathbf{C}_b^n(\psi, \theta, \phi) = \begin{bmatrix} 1 & -\psi & \theta \\ \psi & 1 & -\phi \\ -\theta & \phi & 1 \end{bmatrix} \tag{49}$$

Wings level constant altitude flight conditions dictate the nominal $\mathbf{C}_b^n = \mathbf{I}_3$ from which the perturbation of $\mathbf{C}_b^n$ can be solved

$$\delta\mathbf{C}_b^n = \begin{bmatrix} 0 & -\delta\psi & \delta\theta \\ \delta\psi & 0 & -\delta\phi \\ -\delta\theta & \delta\phi & 0 \end{bmatrix} \tag{50}$$

The derivative of the body to navigation frame DCM, $\mathbf{C}_b^n$, is dependent on the rate of body rotation, and the rate of the navigation frame rotation. Due to no body rotations in a wings level flight scenario, the body frame and navigation frame alignment remains constant. Reducing Equation (51) to the constant DCM in Equation (2)

$$\begin{aligned}\dot{\mathbf{C}}_b^n &= \mathbf{C}_b^n \boldsymbol{\Omega}_{ib}^{(b)} - \boldsymbol{\Omega}_{in}^{(n)} \mathbf{C}_b^n \\ \dot{\mathbf{C}}_b^n &= 0\end{aligned} \tag{51}$$

Misalignment angles of a notional platform system which is mechanized to the navigation frame is expressed as

$$\delta\boldsymbol{\Psi} = -\delta\mathbf{C}_b^n \mathbf{C}_n^b \tag{52}$$

where $\delta\boldsymbol{\Psi}$ is the skew symmetric form of the angular errors vector $\delta\boldsymbol{\psi}$, ie.,

$$\delta\boldsymbol{\Psi} = \delta\boldsymbol{\psi}\times \tag{53}$$

Referring to Equation (52), the angular errors can be calculated. Keeping in mind, the Euler angles of the aircraft are assumed zero in the nominal $\mathbf{C}_b^n$.

$$\begin{aligned}\delta\boldsymbol{\Psi} &= -\begin{bmatrix} 0 & -\delta\psi & \delta\theta \\ \delta\psi & 0 & -\delta\phi \\ -\delta\theta & \delta\phi & 0 \end{bmatrix} \begin{bmatrix} 1 & \psi & -\theta \\ -\psi & 1 & \phi \\ \theta & -\phi & 1 \end{bmatrix} \\ \delta\boldsymbol{\Psi} &= -\begin{bmatrix} \delta\psi\cdot\psi + \delta\theta\cdot\theta & -\delta\psi - \delta\theta\cdot\phi & -\delta\psi\cdot\phi + \delta\theta \\ \delta\psi - \delta\phi\cdot\theta & \delta\psi\cdot\psi + \delta\phi\cdot\phi & -\delta\psi\cdot\theta - \delta\phi \\ -\delta\theta - \delta\phi\cdot\psi & -\delta\theta\cdot\psi + \delta\phi & \delta\theta\cdot\theta + \delta\phi\cdot\phi \end{bmatrix}\end{aligned} \tag{54}$$

Substituting the Euler angle values from the nominal $\mathbf{C}_b^n = \mathbf{I}_3$, the angular errors matrix $\delta\boldsymbol{\Psi}$ is

$$\delta\boldsymbol{\Psi} = \begin{bmatrix} 0 & \delta\psi & -\delta\theta \\ -\delta\psi & 0 & \delta\phi \\ \delta\theta & -\delta\phi & 0 \end{bmatrix} \tag{55}$$

In vector form, the angular errors can be extracted using Equation (53) yielding Equation (56). Following convention, negative angular errors is not regular practice and the negative will be relegated to the other multiplicand.

$$\delta\boldsymbol{\psi} = \begin{bmatrix} -\delta\phi & -\delta\theta & -\delta\psi \end{bmatrix}^T \tag{56}$$

Velocity error equation dynamics are expressed referencing Section 2.4. Over short flight distances, that is, during an INS aiding session, the velocity error equation dynamics are simplified to the specific force vector rotated by the error in angles $\boldsymbol{\Psi}$ plus the effect of the accelerometer biases.

$$\begin{aligned} \delta\dot{\mathbf{v}}^{(n)} = \; & [\mathbf{f}^{(n)}\times]\boldsymbol{\psi} + \mathbf{C}_b^n\delta\mathbf{f}^{(b)} - (2\omega_{ie}^n + \omega_{en}^n)\times\delta\mathbf{v} \\ & - (2\delta\omega_{ie}^n + \delta\omega_{en}^n)\times\mathbf{v} - \delta\mathbf{g} \end{aligned}$$

Equation (57) shows the simplified velocity error dynamics implemented in this research with the elimination terms accounting for the rotation of the Earth, and error in gravity.

$$\delta\dot{\mathbf{v}}^{(n)} = [\mathbf{f}^{(n)}\times]\boldsymbol{\psi} + \mathbf{C}_b^n\delta\mathbf{f}^{(b)} \tag{57}$$

The skew symmetric specific force matrix is derived from the flight conditions in Section 3.2. Constant altitude, winds level flight along the x_n direction generating a specific force vector with only gravitational components in the z_n axis and acceleration force in the x_n. Theoretically, no forces will be observed in the y_n axis in the developed navigation scenario. The specific force vector in Equation (58) is populated according to the convention of body forces minus the gravitational forces, keeping in mind the ENU reference frame convention.

$$\mathbf{f}^{(n)} = \begin{pmatrix} f_x^{(n)} \\ f_y^{(n)} \\ f_z^{(n)} \end{pmatrix} = \begin{pmatrix} a_x \\ 0 \\ 0 \end{pmatrix} - \begin{pmatrix} 0 \\ 0 \\ -g \end{pmatrix} = \begin{pmatrix} a_x \\ 0 \\ g \end{pmatrix} \tag{58}$$

Therefore, the skew symmetric matrix form of the specific force vector becomes

$$\mathbf{f}^{(n)}\times = \mathbf{F}^{(n)} = \begin{bmatrix} 0 & -g & 0 \\ g & 0 & -a_x \\ 0 & a_x & 0 \end{bmatrix} \tag{59}$$

The rate of change in position error $\delta\dot{\mathbf{p}}^{(n)}$ is defined as the error in velocity $\delta\mathbf{v}^{(n)}$.

$$\delta\dot{\mathbf{p}}^{(n)} = \delta\mathbf{v}^{(n)} \tag{60}$$

Referencing Equation (47), the navigation state error dynamics matrix $\mathbf{A}$ and the input matrix $\mathbf{\Gamma}$ in Equation (61) are formed from the INS error equations developed in this section.

$$\delta\dot{\mathbf{x}} = \begin{bmatrix} \mathbf{0_3} & \mathbf{I_3} & \mathbf{0_3} \\ \mathbf{0_3} & \mathbf{0_3} & -\mathbf{F}^{(n)} \\ \mathbf{0_3} & \mathbf{0_3} & \mathbf{0_3} \end{bmatrix} \delta\mathbf{x} + \begin{bmatrix} \mathbf{0_3} & \mathbf{0_3} \\ \mathbf{C}_b^n & \mathbf{0_3} \\ \mathbf{0_3} & \mathbf{C}_b^n \end{bmatrix} \delta\mathbf{u} \tag{61}$$

Where $\mathbf{F}^{(n)}$ is the skew symmetric specific force matrix from Equation (59) and $\mathbf{C}_b^n = \mathbf{I}_3$ as the nominal DCM transformation from the body frame to the navigation reference frame.

Due to the presence of accelerometer and gyroscope biases, bias error states are incorporated into the system by way of augmentation. The sensor bias errors are modeled as Gaussian distributed random variables described with mean (μ) and standard deviation (σ). The accelerometer bias errors $\delta f^{(b)}$ and the gyroscope bias errors $\delta\omega^{(b)}$

in the body frame are described as

$$\begin{aligned} \delta \boldsymbol{f}^{(b)} &\sim N(0, \sigma_{b_a}^2) \\ \delta \boldsymbol{\omega}^{(b)} &\sim N(0, \sigma_{b_g}^2) \end{aligned} \tag{62}$$

The navigation state error vector is augmented with the accelerometer and gyroscope biases according to

$$\delta \mathbf{x} = \begin{bmatrix} \delta \mathbf{p}^{(n)}, & \delta \mathbf{v}^{(n)}, & \delta \boldsymbol{\psi}, & \delta \mathbf{f}^{(b)}, & \delta \boldsymbol{\omega}^{(b)} \end{bmatrix}^T \tag{63}$$

as well as the dynamics matrix which becomes a 15×15 matrix.

$$\mathbf{A} = \begin{bmatrix} \mathbf{0_3} & \mathbf{I_3} & \mathbf{0_3} & \mathbf{0_3} & \mathbf{0_3} \\ \mathbf{0_3} & \mathbf{0_3} & -\mathbf{F}^{(n)} & \mathbf{C}_b^n & \mathbf{0_3} \\ \mathbf{0_3} & \mathbf{0_3} & \mathbf{0_3} & \mathbf{0_3} & \mathbf{C}_b^n \\ \mathbf{0_3} & \mathbf{0_3} & \mathbf{0_3} & \mathbf{0_3} & \mathbf{0_3} \\ \mathbf{0_3} & \mathbf{0_3} & \mathbf{0_3} & \mathbf{0_3} & \mathbf{0_3} \end{bmatrix}_{15 \times 15} \tag{64}$$

Referring back to the state space stochastic model, Section 2.6, the noise input matrix $\mathbf{G}$ is formed to add noise accordingly. In the case of a constant random bias error, no input noise in necessary.

$$\mathbf{G} = \begin{bmatrix} \mathbf{0_3} & \mathbf{0_3} \\ \mathbf{C}_b^n & \mathbf{0_3} \\ \mathbf{0_3} & \mathbf{C}_b^n \\ \mathbf{0_3} & \mathbf{0_3} \\ \mathbf{0_3} & \mathbf{0_3} \end{bmatrix}_{15 \times 6} \tag{65}$$

Therefore, the state space stochastic model is newly defined accounting for accelerometer and gyroscope biases by way of augmentation. Due to the implementation of

random constant biases, the inclusion of the noise input matrix and noise strength matrix is not needed. Modeling of biases as FOGM processes and the addition of INS drift would require the use of the noise input matrix and noise strength matrix [14].

Incorporation of a barometric altimeter sensor bias is incorporated because of the sensitivity of the z channel and the standard accompaniment of an altitude aiding sensor with a navigation quality INS. The complete state space system model implemented in this research is

$$\delta\dot{\mathbf{x}} = \begin{bmatrix} \mathbf{0_3} & \mathbf{I_3} & \mathbf{0_3} & \mathbf{0_3} & \mathbf{0_3} & 0 \\ \mathbf{0_3} & \mathbf{0_3} & -\mathbf{F}^{(n)} & \mathbf{C}_b^n & \mathbf{0_3} & 0 \\ \mathbf{0_3} & \mathbf{0_3} & \mathbf{0_3} & \mathbf{0_3} & -\mathbf{C}_b^n & 0 \\ \mathbf{0_3} & \mathbf{0_3} & \mathbf{0_3} & \mathbf{0_3} & \mathbf{0_3} & 0 \\ \mathbf{0_3} & \mathbf{0_3} & \mathbf{0_3} & \mathbf{0_3} & \mathbf{0_3} & 0 \\ 0 & 0 & 0 & 0 & 0 & 0 \end{bmatrix} \begin{bmatrix} \delta\mathbf{p}^{(n)} \\ \delta\mathbf{v}^{(n)} \\ \delta\boldsymbol{\psi} \\ \delta\mathbf{f}^{(b)} \\ \delta\boldsymbol{\omega}^{(b)} \\ \delta b_{baro}^{(b)} \end{bmatrix} \tag{66}$$

The initialized covariance matrix associated with the augmented state model shown in Equation (67) assumes a perfect initial INS alignment and known information from of the INS bias sources from the manufacture specifications.

$$\mathbf{P}_0 = \begin{bmatrix} \mathbf{0}_3 & \mathbf{0}_3 & \mathbf{0}_3 & \mathbf{0}_3 & \mathbf{0}_3 & \mathbf{0} \\ \mathbf{0}_3 & \mathbf{0}_3 & \mathbf{0}_3 & \mathbf{0}_3 & \mathbf{0}_3 & \mathbf{0} \\ \mathbf{0}_3 & \mathbf{0}_3 & \mathbf{0}_3 & \mathbf{0}_3 & \mathbf{0}_3 & \mathbf{0} \\ \mathbf{0}_3 & \mathbf{0}_3 & \mathbf{0} & \sigma_{b_a}^2 & \mathbf{0}_3 & \mathbf{0} \\ \mathbf{0}_3 & \mathbf{0}_3 & \mathbf{0}_3 & \mathbf{0}_3 & \sigma_{b_g}^2 & \mathbf{0} \\ \mathbf{0} & \mathbf{0} & \mathbf{0} & \mathbf{0} & \mathbf{0} & \sigma_{b_b}^2 \end{bmatrix}_{16\times 16} \tag{67}$$

3.3 Method 1: Driftmeter Replication

This section will outline the simulations performed to validate assumptions made about use of the dritmeter. Capturing the aiding action the driftmeter provided is simulated using both structured steady-state fight dynamics and flight dynamics with acceleration inputs in the direction of travel. The measurement model is derived as linear. Implementation of the KF used to replicate the navigator's driftmeter measurements will also be covered.

INS Error Model Robustness.

With a simplified wings level INS error model, it was prudent to test how robust the INS error model was to dynamic flight conditions rather than just steady-state flight conditions. Therefore, robustness testing of the INS error model was simulated to determine how acceleration forces versus constant velocity flight impact INS error accumulation. The definition of the error state model indicates that acceleration in the direction of travel will yield minute differences in navigation state error results but the investigation is warranted.

Input acceleration forces to simulate acceleration or deceleration of the aircraft during flight in the x_n direction changed the state transition matrix $\mathbf{\Phi}_d$ from being constant to becoming time-dependent $\mathbf{\Phi}_{d_{k+1}}$. Referencing Equation (58), a sine wave function was used to generate the acceleration and deceleration forces to drive the flight dynamics.

$$\mathbf{f}^{(n)} = \begin{pmatrix} f_x^{(n)} \\ f_y^{(n)} \\ f_z^{(n)} \end{pmatrix} = \begin{pmatrix} \frac{a_x}{g} \sin \omega t \\ 0 \\ 0 \end{pmatrix} - \begin{pmatrix} 0 \\ 0 \\ -g \end{pmatrix} = \begin{pmatrix} \frac{a_x}{g} \sin \omega t \\ 0 \\ g \end{pmatrix} \tag{68}$$

The magnitude of the acceleration force input a_x is non-dimensionalized with the

force of gravity g. Acceleration input frequency ω was empirically tested to determine the the highest degree of INS error model impact as high frequency repeating inputs appeared to cancel out over the course of flight.

Robustness of the INS error model in the direction of travel will be simulated through the parameters in Table 3.

Table 3. Steady-State Flight Constants

$\frac{a}{g}$	$\omega(\frac{rad}{s})$
0.2	0.005
0.4	0.05
0.6	0.5
0.8	1
1.0	

Measurement Model - Measurement Equation.

Referencing Section 3.2, the measurement model for World War II navigator's driftmeter operations will be constructed in this section. The history of the driftmeter in Section 2.5 outlines the measurements the navigator used to calculate the ground speed and the wind vector. Essentially, the navigator was able to get a velocity estimate as the aircraft was on autopilot traveling at constant airspeed. With a measurement of velocity, the navigator could determine $\delta\mathbf{v}$. Therefore, the measurement model used to replicate the navigator's operation of the dirftmeter is a linear model that taps δv_x.

Utilizing the barometric sensor to stabilize the z channel, the barometric altimeter measurement is constructed via substitution shown in Equation (69). Subtracting the output of the INS, z_c from the output of the barometric sensor, z_{baro} yields the error

in the z channel.

$$\begin{aligned} \bar{z} &= z_c - z_{baro} \\ \bar{z} &= (z + \delta z) - (z + \delta b_{baro}) \end{aligned} \tag{69}$$

Kalman filter measurements are defined as the difference between the INS velocity output v_{x_c} and the driftmeter velocity output v_{x_m}; and the difference between the the INS altitude output z_c and the barometric altimeter sensor output z_{baro}. Equation (70) shows the measurement given to the KF.

$$\bar{\mathbf{z}}_{k+1} = \begin{pmatrix} v_{x_c} - v_{x_m} \\ z_c - z_{baro} \end{pmatrix} \tag{70}$$

By substitution, the measurement given to the KF can be expressed in error terms. The velocity error in the INS is δv_x, and the error in the driftmeter measurement is due to the optical device, δx_f. The INS error in altitude is δz and the error in the barometric altimeter measurement is δb_{baro}, from Equation (69).

$$\bar{\mathbf{z}}_{k+1} = \begin{pmatrix} \delta v_x - 2\delta x_f \\ \delta z - \delta b_{baro} \end{pmatrix} \tag{71}$$

The measurement covariance $\mathbf{R}$, the uncertainty associated with the measurements given to the KF, is derived as Equation (72). Error associated with the track of the ground feature through the sighting device of the driftmeter is σ_c. No human induced timing or feature tracking error is considered.

$$\mathbf{R} = \begin{bmatrix} \sigma_{baro}^2 + \frac{2}{\Delta t^2}\sigma_c^2 & 0 \\ 0 & \sigma_{baro}^2 \end{bmatrix} \tag{72}$$

The linear measurement matrix for the measurement given to the KF, $\mathbf{H}$, repli-

cates the navigator's driftmeter measurements and the use of a barometric altitude aiding sensor. Also known as the observation matrix, $\mathbf{H}$ is shown in Equation (73).

$$\mathbf{H} = \begin{bmatrix} 0 & 0 & 0 & 1 & 0 & 0 & 0 & 0 & 0 & 0 & 0 & 0 & 0 & 0 & 0 & -1 \end{bmatrix} \tag{73}$$

Using the measurement model developed in this section, the use of a Kalman filter can be used to estimate the INS error in velocity and altitude during a measurement epoch. Navigator's did not continuously use the driftmeter as a constant measurement source. Rather, it was used intermittently for course correction while dead reckoning when operationally available.

Kalman Filter.

Use of the Kalman filter will provide an estimate of the error in velocity and error in altitude which can be used to correct the INS. In the navigator's time, error models currently used as community standards were not utilized in flight. However, with knowledge of the INS quality, the navigator could calculate an estimate of the error covariance using flight time. Therefore, a comparison will be drawn between initializing the Kalman filter with independent covariance terms and zeroing out all cross-covariance terms versus initialization with the full $free$ INS covariance.

In the scenario when the Kalman filter is initialized with the independent covariances and no cross-covariance terms, the covariance matrix $\mathbf{P}_0^+$ would be set to Equation (74). With only knowledge about the individual decoupled performance of the sensors, a time propagation of the uncertainty is possible.

$$\mathbf{P}_0^+ = \begin{bmatrix} \mathbf{P}_{k(1,1)}^{+\ (free)} & \mathbf{0} & \mathbf{0} & \mathbf{0} & \mathbf{0} \\ \mathbf{0} & \ddots & \mathbf{0} & \mathbf{0} & \mathbf{0} \\ \mathbf{0} & \mathbf{0} & \ddots & \mathbf{0} & \mathbf{0} \\ \mathbf{0} & \mathbf{0} & \mathbf{0} & \ddots & \mathbf{0} \\ \mathbf{0} & \mathbf{0} & \mathbf{0} & \mathbf{0} & \mathbf{P}_{k(16,16)}^{+\ (free)} \end{bmatrix} \tag{74}$$

Utilizing the cross-covariance terms that are generated because of the state transition matrix, $\mathbf{\Phi}_d$, allows measurements of a state to affect another correlated state. In control theory, observability indicates whether a state can be calculated from the output [11]. State correlation from cross-covariance relationships can result in observability of states that are not directly incorporated in the measurement model. Initialization of the Kalman filter with the cross-covariance terms results in correlation of position, velocity, and accelerometer bias states for respective axes. The initial covariance matrix with correlation is Equation (75).

$$\mathbf{P}_0^+ = \mathbf{P}_k^{+\ (free)} \tag{75}$$

The Kalman filter propagate, update, and Kalman gain equations are show in Equations (76), (77), and (78).

$$\begin{aligned} \delta\hat{\mathbf{x}}_{k+1}^- &= \mathbf{\Phi}\delta\hat{\mathbf{x}}_k^+ \quad , \delta\hat{\mathbf{x}}_0^+ = 0 \\ \mathbf{P}_{k+1}^- &= \mathbf{\Phi}\mathbf{P}_k^+\mathbf{\Phi}^T + \mathbf{Q}_d \quad , \mathbf{P}_0^+ = \mathbf{P}_k \ (free \text{ INS}) \end{aligned} \tag{76}$$

$$\mathbf{K}_{k+1} = \mathbf{P}_{k+1}^-\mathbf{H}^T(\mathbf{H}\mathbf{P}_{k+1}^-\mathbf{H}^T + \mathbf{R})^{-1} \tag{77}$$

$$\begin{aligned} \delta\hat{\mathbf{x}}_{k+1}^+ &= \delta\hat{\mathbf{x}}_{k+1}^- + \mathbf{K}_{k+1}(\bar{\mathbf{z}}_{k+1} - \mathbf{H}\delta\hat{\mathbf{x}}_{k+1}^-) \\ \mathbf{P}_{k+1}^+ &= (\mathbf{I} - \mathbf{K}_{k+1}\mathbf{H})\mathbf{P}_{k+1}^- \quad , k = 0, 1, ..., L-1 \end{aligned} \tag{78}$$

At the end of a measurement epoch, the Kalman filter estimate $\delta\hat{\mathbf{x}}$ will be used to reset the INS to capture the resultant aiding action native to the inertial system. The INS will be reset by subtracting the Kalman filter estimate of the navigation state error and setting the INS error covariance to the Kalman filter covariance.

$$\delta\mathbf{x}_{k+1} = \delta\mathbf{x}_{k+1} - \delta\hat{\mathbf{x}}^{+}_{k+1} \tag{79}$$

$$\mathbf{P}^{(\text{ins})}_{k+1} = \mathbf{P}^{+}_{k+1} \tag{80}$$

3.4 Method 2: Contemporary Driftmeter

The contemporary driftmeter is the implementation of the driftmeter measurements the navigator used but accomplished with current technology. Use of a more realistic measurement model rather than a theoretical observation matrix translates the information available from an INS and E/O system to measurements that can be used by the Kalman filter to estimate the navigation state error. There are similar elements of the Navigator Replication simulation development that exist in the Contemporary Dritmeter simulation.

Measurement Model - Measurement Equation.

A measurement epoch is the time the aircraft is in autopilot mode and the stationary ground feature is tracked by the pilot while in the E/O system's field of view. It is during a measurement epoch, that INS aiding action will take place. At the conclusion of the INS aiding session, the INS will be reset. Figure 20 pictorially shows the geolocation and then tracking of a ground feature through one measurement epoch.

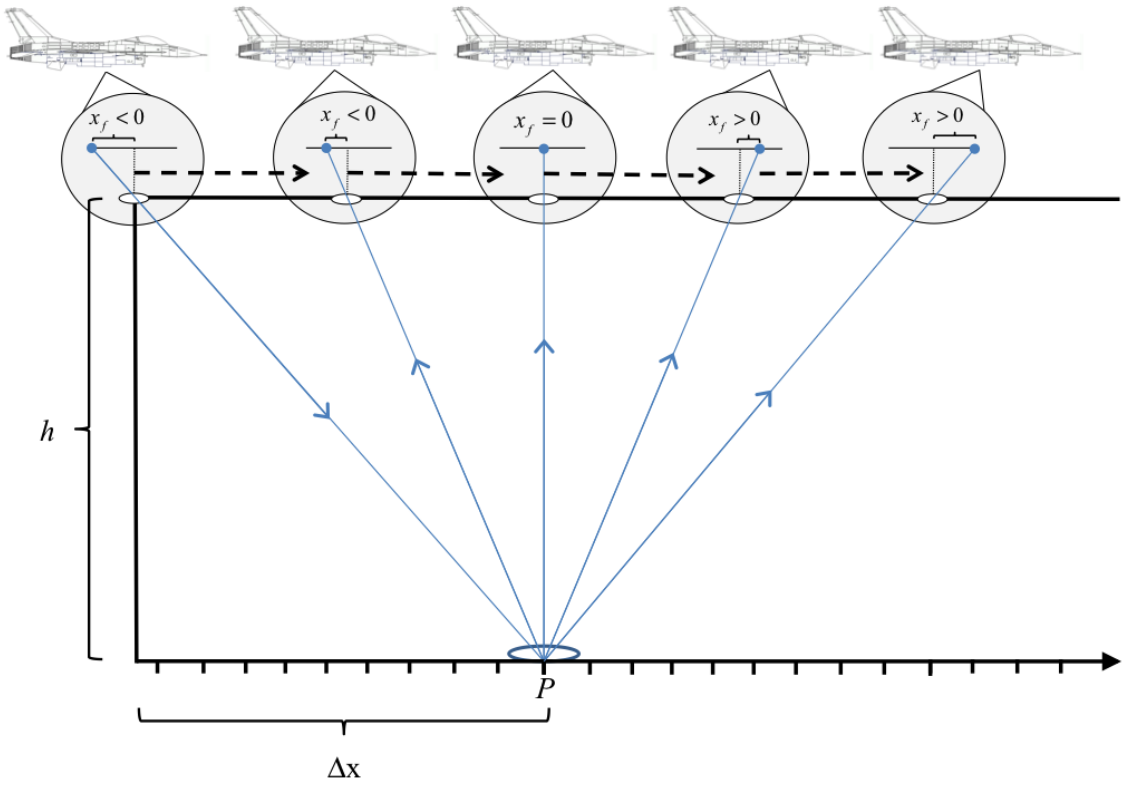

Figure 20. Pilot Geolocating and Then Tracking a Ground Feature (P) Through a Measurement Epoch

A relationship of similar triangles generated from Section 3.2 is invoked between the image location in the inverted image plane and ground feature location in the reference frame. The relationship is dependent on the knowledge of both the E/O system's focal length f and ground feature elevation - see Figure 19. The similar triangle relationship allows the construction of the measurement equation shown in Equation (81) [18].

$$\begin{pmatrix} x_p \\ y_p \\ z_p \end{pmatrix} = \begin{pmatrix} x \\ y \\ z \end{pmatrix} + \frac{|R_{LOS}|}{\sqrt{x_f^2 + y_f^2 + f^2}} \mathbf{C}_b^n \begin{pmatrix} x_f \\ y_f \\ -f \end{pmatrix} \tag{81}$$

This nonlinear measurement equation ties together the *true* navigation state, the

"known" position of the ground feature, and the *true* ground feature bearing measurements coming from the E/O system. Equation (81) represents two independent measurements: with the elevation of the ground feature z_p known from terrain data, the three measurement equations can be reduced to two independent nonlinear measurement equations [16]:

$$\begin{pmatrix} x_p \\ y_p \end{pmatrix} = \begin{pmatrix} x \\ y \end{pmatrix} + \frac{z_p - z}{\begin{pmatrix} 0 & 0 & 1 \end{pmatrix} \mathbf{C}_b^n \begin{pmatrix} x_f \\ y_f \\ -f \end{pmatrix}} \begin{bmatrix} 1 & 0 & 0 \\ 0 & 1 & 0 \end{bmatrix} \mathbf{C}_b^n \begin{pmatrix} x_f \\ y_f \\ -f \end{pmatrix} \tag{82}$$

Equation (82) represents two nonlinear measurement equations derived from Equation (81), relating the true aircraft position (x, y, z), true driftmeter measurements (x_f, y_f), and the true ground feature position (x_p, y_p, z_p).

In the derivation of the KF equations it is assumed that the position (x_p, y_p, z_p) of the ground feature P is known. The latter is the geolocated position of the ground feature at the beginning of the measurement epoch, which is calculated also using the two nonlinear Equation (82).

The two nonlinear measurement equations from Equation (82) are linearized and used to derive the measurement matrix $\mathbf{H}_{k+1}$ used in the KF. Equation (82) is also used in the calculation of the measurement that is fed to the KF. The measurement fed to the KF, $\bar{\mathbf{z}}_{k+1}$, is corrupted with INS and E/O system errors. Specifically, measurements brought into the Kalman Filter are defined as the difference between the measured position of the ground feature and the "*known*" position of the geolocated ground feature. The KF measurements ($\bar{\mathbf{z}}_{k+1}$) are the difference of the geolocated ground features' position at the beginning of the measurement epoch and the ground feature position calculated using subsequent bearing measurements taken throughout the measurement epoch. This embodies the optical information provided by a drift-

meter, and is given to the KF as its measurements, $\bar{\mathbf{z}}_{k+1}$, to be fused with the inertial measurements.

A measurement epoch extends through the discrete time instants $k = 1, ..., L$. At time $k = 0$, before the measurement epoch, the ground feature is geolocated, that is, its coordinates (x_{p_m}, y_{p_m}) are calculated according to Equation (83). The true navigation state of the aircraft on the Right Hand Side (RHS) of Equation (82) is substituted with the INS output which is corrupted with INS errors. The INS output is designated with the subscript c. Also, on the RHS of Equation (82), the true image plane pixel location $\binom{x_f}{y_f}$ of the ground feature is substituted with the E/O system measurement of the ground feature. The E/O system contains measurement errors, $\binom{\delta x_f}{\delta y_f}$. Measurements from the E/O system are designated with the m subscript.

$$\begin{pmatrix} x_{p_m} \\ y_{p_m} \end{pmatrix} = \begin{pmatrix} x_c \\ y_c \end{pmatrix} + \frac{z_p - z_c}{\begin{pmatrix} 0 & 0 & 1 \end{pmatrix} (\mathbf{C}_b^n)_c \begin{pmatrix} x_{f_m} \\ y_{f_m} \\ -f \end{pmatrix}} \begin{bmatrix} 1 & 0 & 0 \\ 0 & 1 & 0 \end{bmatrix} (\mathbf{C}_b^n)_c \begin{pmatrix} x_{f_m} \\ y_{f_m} \\ -f \end{pmatrix} \tag{83}$$

The *"known"* coordinates $\binom{x_{p_m}}{y_{p_m}}$ of the geolocated ground feature are used throughout the rest of the measurement epoch. The measurement $\bar{\mathbf{z}}_{k+1}$ given to the KF is the geolocated ground feature throughout the epoch at time $k = 1, ..., L$ generated using the *calculated* (x_c, y_c, z_c) from the INS and x_{f_m}, y_{f_m} provided by the E/O system minus the position of the geolocated ground feature at time $l = 0$, computed using the *calculated* (x_c, y_c, z_c) also from the INS, and x_{f_m}, y_{f_m} provided by the E/O system.

Thus, the same measurement model in Equation (83) is used to first geolocate the ground feature at time $k = 0$ yielding $\binom{x_{p_m}}{y_{p_m}}$ and then calculate the ground feature position at time $k = 1, 2, ...L$ throughout the measurement epoch yielding $\binom{x_{p_c}}{y_{p_c}}_k$. In summary, calculated values are provided by the INS and are denoted by

the subscript c, namely (x_c, y_c, z_c) which is the aircraft position containing INS errors $(\delta\mathbf{p}, \delta\mathbf{v}, \delta\Psi)$. The measurements from the E/O system are (x_{f_m}, y_{f_m}), corrupted with Gaussian distributed pixel location errors $\delta x_f, \delta y_f$. The measurement $\bar{\mathbf{z}}_{k+1}$ given to the Kalman Filter is displayed in Equation (84).

$$\bar{\mathbf{z}}_{k+1} \triangleq \begin{pmatrix} x_{p_c} \\ y_{p_c} \end{pmatrix}_k - \begin{pmatrix} x_{p_m} \\ y_{p_m} \end{pmatrix}_{k=0} , k = 1, ..., L \tag{84}$$

The rationale for this approach is as follows. For the purpose of deriving the KF, which operates at time $k = 1, 2, ..., L$, the position of the ground feature on the Left Hand Side (LHS) of Equation (82) at time $k = 1, 2..., L$ is taken to be *"known"*. At the same time, the position (x, y, z) of the aircraft on the RHS of Equation (82) is perturbed:

$$\begin{aligned} x &= x_c - \delta x \\ y &= y_c - \delta y \\ z &= z_c - \delta z \end{aligned} \tag{85}$$

Following the convention of perturbing the position of the aircraft (x, y, z), the body to navigation frame DCM can be perturbed according to Equation (86)

$$I = \mathbf{C}_b^n = (\mathbf{C}_b^n)_c - \delta\mathbf{C}_b^n \tag{86}$$

With all terms on the RHS of the equation perturbed and now expressed in error quantities, subtraction of the two nonlinear equations made from Equation (82) yields a linearized measurement equation.

Linearization of the Measurement Equation.

$$
\begin{aligned}
\bar{\mathbf{z}}_{k+1} = &\begin{pmatrix} \delta x \\ \delta y \end{pmatrix} - \frac{1}{\begin{pmatrix} 0 & 0 & 1 \end{pmatrix} (\mathbf{C}_b^n)_c \begin{pmatrix} x_{f_m} \\ y_{f_m} \\ -f \end{pmatrix}} \begin{bmatrix} 1 & 0 & 0 \\ 0 & 1 & 0 \end{bmatrix} (\mathbf{C}_b^n)_c \begin{pmatrix} x_{f_m} \\ y_{f_m} \\ -f \end{pmatrix} \delta z \\
&+ \frac{z_p - z_c}{\begin{pmatrix} 0 & 0 & 1 \end{pmatrix} (\mathbf{C}_b^n)_c \begin{pmatrix} x_{f_m} \\ y_{f_m} \\ -f \end{pmatrix}} \begin{bmatrix} 1 & 0 & 0 \\ 0 & 1 & 0 \end{bmatrix} \begin{bmatrix} 0 & -\delta\psi & \delta\theta \\ \delta\psi & 0 & -\delta\phi \\ -\delta\theta & \delta\phi & 0 \end{bmatrix} \begin{pmatrix} x_{f_m} \\ y_{f_m} \\ -f \end{pmatrix} \\
&- \frac{z_p - z_c}{[\begin{pmatrix} 0 & 0 & 1 \end{pmatrix} (\mathbf{C}_b^n)_c \begin{pmatrix} x_{f_m} \\ y_{f_m} \\ -f \end{pmatrix}]^2} \begin{pmatrix} 0 & 0 & 1 \end{pmatrix} \begin{bmatrix} 0 & -\delta\psi & \delta\theta \\ \delta\psi & 0 & -\delta\phi \\ -\delta\theta & \delta\phi & 0 \end{bmatrix} \begin{pmatrix} x_{f_m} \\ y_{f_m} \\ -f \end{pmatrix} \begin{bmatrix} 1 & 0 & 0 \\ 0 & 1 & 0 \end{bmatrix} (\mathbf{C}_b^n)_c \begin{pmatrix} x_{f_m} \\ y_{f_m} \\ -f \end{pmatrix} \\
&+ \frac{z_p - z_c}{\begin{pmatrix} 0 & 0 & 1 \end{pmatrix} (\mathbf{C}_b^n)_c \begin{pmatrix} x_{f_m} \\ y_{f_m} \\ -f \end{pmatrix}} \begin{bmatrix} 1 & 0 & 0 \\ 0 & 1 & 0 \end{bmatrix} (\mathbf{C}_b^n)_c \begin{pmatrix} \delta x_f \\ \delta y_f \\ 0 \end{pmatrix} \\
&- \frac{z_p - z_c}{[\begin{pmatrix} 0 & 0 & 1 \end{pmatrix} (\mathbf{C}_b^n)_c \begin{pmatrix} x_{f_m} \\ y_{f_m} \\ -f \end{pmatrix}]^2} \begin{pmatrix} 0 & 0 & 1 \end{pmatrix} (\mathbf{C}_b^n)_c \begin{pmatrix} \delta x_f \\ \delta y_f \\ 0 \end{pmatrix} \begin{bmatrix} 1 & 0 & 0 \\ 0 & 1 & 0 \end{bmatrix} (\mathbf{C}_b^n)_c \begin{pmatrix} x_{f_m} \\ y_{f_m} \\ -f \end{pmatrix}, k = 1, 2, ..., L
\end{aligned}
\tag{87}
$$

Simplification of terms in Equation (87) yields the linearized measurement model, that is, the observation matrix $\mathbf{H}_{k+1}$ in Equation (88). The values contained in the $\mathbf{H}_{k+1}$ matrix are the *true* nominal variables and determined by the autopilots settings. The time dependent observation matrix at time k, which can be augmented with $0_{3\times 6}$ to account for the accelerometers' and gyros' biases and augmented with $\begin{pmatrix} 0 & 0 & -1 \end{pmatrix}^T$ to account for the barometric altimeter sensor random constant bias is

$$
\mathbf{H}_{k+1} = \begin{bmatrix}
1 & 0 & \frac{x_f}{f} & 0 & 0 & 0 & -(z_p - z)\frac{x_f}{f}\frac{y_f}{f} & (z_p - z)[(\frac{x_f}{f})^2 + 1] & (z_p - z)\frac{y_f}{f} & 0 & 0 & 0 & 0 & 0 & 0 & 0 \\
0 & 1 & \frac{y_f}{f} & 0 & 0 & 0 & -(z_p - z)[1 + (\frac{y_f}{f})^2] & (z_p - z)\frac{x_f}{f}\frac{y_f}{f} & -(z_p - z)\frac{x_f}{f} & 0 & 0 & 0 & 0 & 0 & 0 & 0 \\
0 & 0 & 1 & 0 & 0 & 0 & 0 & 0 & 0 & 0 & 0 & 0 & 0 & 0 & 0 & -1
\end{bmatrix}
\tag{88}
$$

The 3rd row in the $\mathbf{H}_{k+1}$ matrix allows for the inclusion of an independent altitude measurement, in this case a barometric altimeter sensor is used. The measurement noise variance $\mathbf{R}$ is provided in Equation (89) and is determined by the Gaussian distributed noise associated with the pixel location of a feature from the scene in a CCD camera [2]. The covariance matrix of the measurement error needed in the KF is

$$\mathbf{R} = \begin{bmatrix} \frac{\sigma_c^2}{f^2}(z_p - z)^2 & 0 & 0 \\ 0 & \frac{\sigma_c^2}{f^2}(z_p - z)^2 & 0 \\ 0 & & \sigma_{baro} \end{bmatrix} \tag{89}$$

where σ_{baro} is the barometric altimeter sensor measurement error standard deviation.

The time dependent $\mathbf{H}_{k+1}$ matrix and the $\mathbf{R}$ matrix define the linear measurement model relating the E/O system outputs x_f and y_f to the INS navigation state errors.

Altitude Aiding: Barometric Altimeter Measurement.

Incorporating an altitude aiding sensor is necessary with the use of a navigation grade inertial system [10]. Typically, the altitude aiding sensor of choice is a barometric altimeter which preserves the passive nature of the inertial system as opposed to a radar altimeter. The barometric altimeter will measure the altitude of the aircraft above a fixed calibrated level which is provided by a ground based system. Because the barometric pressure of mercury is measured to the hundredth inch, there will be a bias that exists in the barometric altimeter measurement. Referencing the Honeywell AM-250 [9], with accuracy of ± 0.01 $in Hg$, $1 Hg$ at $0^\circ \approx 2.67$ m at 0°. This research will use a non-dimensionalized barometric altimeter measurement $\sigma_{baro} = \frac{1\ m}{1000\ m} = 0.001$.

The barometric altimeter measurement model requires the addition of a measure-

ment bias. The incorporation of a barometric altimeter bias is accomplished as a constant random Gaussian bias also non-dimensionalized according to $\sigma_{b_{baro}} = \frac{5\ m}{1000\ m} = 0.005$. The sensor measurement model is defined as measuring the true altitude with the inclusion of a barometric altimeter bias.

$$\bar{z}_{baro} = z + \delta b_{baro} \tag{90}$$

Deriving the altitude update measurement $\bar{z}_{baro}$ that is used by the Kalman filter to update the navigation state error vector, is consistent with the linearization technique used to generate the E/O system measurements for the Kalman filter. The error in altitude when incorporating the barometric altimeter will be the INS δz error from the z_c solution minus the barometric altimeter sensor bias, δb_{baro}.

$$\begin{aligned} z_c &= z + \delta z \\ \bar{z} &= z_c - z_{baro} \\ \bar{z} &= (z + \delta z) - (z + \delta b_{baro}) \end{aligned} \tag{91}$$

The constant linear observation matrix $\mathbf{H}(baro)$ is

$$\mathbf{H}(baro) = \begin{bmatrix} 0 & 0 & 1 & 0 & 0 & 0 & 0 & 0 & 0 & 0 & 0 & 0 & 0 & 0 & 0 & -1 \end{bmatrix} \tag{92}$$

which maps the navigation state error vector to measurement space.

Use of the barometric altimeter measurement model is invoked for all time. As opposed to the E/O system measurements which are only available when a ground feature is in the field of view. Therefore, a barometric altimeter sensor measurement will be used to update the INS at every time step. The INS error in altitude, δz, will be constrained by the measurement covariance of the barometric altitude sensor. Correlation will also enable good KF estimates of $\delta \hat{v}_z$ and $\delta \hat{f}_z^{(b)}$ which can be used to

decrease the INS error δv_z and $\delta f_z^{(b)}$.

Kalman Filter.

The barometric altimeter measurement model alone will be used for all time with the exception of the epoch when ground feature measurements are available. Prior to an INS aiding session with E/O system measurements, the observation matrix in Equation (92) is linear and time invariant. When E/O system measurements are used for updating during the epoch, the observation matrix becomes the linear time variant matrix in Equation (88)

Implementation of the Kalman filter during the measurement epoch will provide an estimate of the navigation state error $\delta\mathbf{x}_{k+1}$ and the associated error covariance $\mathbf{P}_{k+1}$. The Kalman filter equations used in Section 3.3 are identical except for the inclusion of a time-dependent observation matrix $\mathbf{H}_{k+1}$ during the measurement epoch where a ground feature is measured with the E/O system.

Due to the ground feature tracking throughout the duration of the measurement epoch, a time-dependent observation matrix must be incorporated into the KF equations. The navigation state error estimate $\mathbf{x}_k$ is propagated forward in time according to Equation (93).

$$\begin{aligned} \delta\hat{\mathbf{x}}_{k+1}^{-} &= \mathbf{\Phi}\delta\hat{\mathbf{x}}_k^{+} \quad , \delta\hat{\mathbf{x}}_0^{+} = 0 \\ \mathbf{P}_{k+1}^{-} &= \mathbf{\Phi}\mathbf{P}_k^{+}\mathbf{\Phi}^T + \mathbf{Q}_d \quad , \mathbf{P}_0^{+} = \mathbf{P}_k \ (free \text{ INS}) \end{aligned} \tag{93}$$

When the measurement epoch begins, $k = 0$, the ground feature is geolocated and no bearing measurements are taken for system update. Starting at time $k = 1$ and continuing until the end of the measurement epoch $k = L$, bearing measurements to the geolocated ground feature are used to update the navigation state error estimate. The Kalman gain is computed similar to Equation (77), but now calculated with the

time-dependent observation matrix $\mathbf{H}_{k+1}$.

$$\mathbf{K}_{k+1} = \mathbf{P}_{k+1}^{-}\mathbf{H}_{k+1}^{T}(\mathbf{H}_{k+1}\mathbf{P}_{k+1}^{-}\mathbf{H}_{k+1}^{T} + \mathbf{R})^{-1} \tag{94}$$

The Kalman filter estimate and covariance using measurements up to time $k+1$ are calculated according to Equation (95), also using the time-dependent observation matrix $\mathbf{H}_{k+1}$.

$$\begin{aligned} \delta\hat{\mathbf{x}}_{k+1}^{+} &= \delta\hat{\mathbf{x}}_{k+1}^{-} + \mathbf{K}_{k+1}(\bar{\mathbf{z}}_{k+1} - \mathbf{H}_{k+1}\delta\hat{\mathbf{x}}_{k+1}^{-}) \\ \mathbf{P}_{k+1}^{+} &= (\mathbf{I} - \mathbf{K}_{k+1}\mathbf{H}_{k+1})\mathbf{P}_{k+1}^{-} \quad , k = 0, 1, ..., L-1 \end{aligned} \tag{95}$$

At the end of the measurement epoch $k = L$, the estimate and covariance computed by the Kalman filter will be used to reset the INS, by subtracting the Kalman filter estimate from the output of the INS like in Equation (79). Keep in mind, the navigation state error estimates are only subtracted from the navigation state error. Specifically, the estimate of the barometric sensor bias is not included in the INS resetting.

$$\delta\mathbf{x}_{k+1} = \delta\mathbf{x}_{k+1} - \delta\hat{\mathbf{x}}_{k+1}^{+} \tag{96}$$

The error covariance capturing how well the filter has estimated the states is carried forward and used to reset the INS error covariance. Resetting the INS error covariance is executed with the same procedure done in Section 3.3 with Equation (80).

$$\mathbf{P}_{k+1}^{(\text{ins})} = \mathbf{P}_{k+1}^{+} \tag{97}$$

Navigation State Kalman Filter.

Reducing the number of states in the Kalman filter increases the observability in the states the KF does estimate. In an attempt to try a new simple technique and move away from potential over modeling, a navigation state Kalman filter is implemented. The KF state vector will only contain the navigation state error ($\delta\mathbf{p}, \delta\mathbf{v}, \delta\boldsymbol{\psi}$) and the barometric altimeter bias ($\delta\mathbf{b}_{baro}$). By excluding the accelerometer and gyroscope biases from the KF state vector, observability is increased.

Also, fixing the position error when entering an INS aiding session and tracking the growth in the velocity error throughout the measurement epoch is key. The KF covariance is initialized according to Equation (98) where the $free$ INS computed covariance is used for all states except for position. Fixing $\delta\mathbf{p}$ at the beginning of an INS aiding session allows the KF to estimate the total error in velocity.

$$\mathbf{P}_0^+ = \begin{bmatrix} \mathbf{0} & \mathbf{0} & \mathbf{0} & \mathbf{P}^{+\ (free)}_{k(1,4)} & \mathbf{P}^{+\ (free)}_{k(1,5)} & \mathbf{P}^{+\ (free)}_{k(1,6)} & \mathbf{P}^{+\ (free)}_{k(1,7)} & \mathbf{P}^{+\ (free)}_{k(1,8)} & \mathbf{P}^{+\ (free)}_{k(1,9)} & \mathbf{P}^{+\ (free)}_{k(1,16)} \\ \mathbf{0} & \mathbf{0} & \mathbf{0} & \mathbf{P}^{+\ (free)}_{k(2,4)} & \mathbf{P}^{+\ (free)}_{k(2,5)} & \mathbf{P}^{+\ (free)}_{k(2,6)} & \mathbf{P}^{+\ (free)}_{k(2,7)} & \mathbf{P}^{+\ (free)}_{k(2,8)} & \mathbf{P}^{+\ (free)}_{k(2,9)} & \mathbf{P}^{+\ (free)}_{k(2,16)} \\ \mathbf{0} & \mathbf{0} & \mathbf{0} & \mathbf{P}^{+\ (free)}_{k(3,4)} & \mathbf{P}^{+\ (free)}_{k(3,5)} & \mathbf{P}^{+\ (free)}_{k(3,6)} & \mathbf{P}^{+\ (free)}_{k(3,7)} & \mathbf{P}^{+\ (free)}_{k(3,8)} & \mathbf{P}^{+\ (free)}_{k(3,9)} & \mathbf{P}^{+\ (free)}_{k(3,16)} \\ \mathbf{P}^{+\ (free)}_{k(4,1)} & \mathbf{P}^{+\ (free)}_{k(4,2)} & \mathbf{P}^{+\ (free)}_{k(4,3)} & \mathbf{P}^{+\ (free)}_{k(4,4)} & \mathbf{P}^{+\ (free)}_{k(4,5)} & \mathbf{P}^{+\ (free)}_{k(4,6)} & \mathbf{P}^{+\ (free)}_{k(4,7)} & \mathbf{P}^{+\ (free)}_{k(4,8)} & \mathbf{P}^{+\ (free)}_{k(4,9)} & \mathbf{P}^{+\ (free)}_{k(4,16)} \\ \mathbf{P}^{+\ (free)}_{k(5,1)} & \mathbf{P}^{+\ (free)}_{k(5,2)} & \mathbf{P}^{+\ (free)}_{k(5,3)} & \mathbf{P}^{+\ (free)}_{k(5,4)} & \mathbf{P}^{+\ (free)}_{k(5,5)} & \mathbf{P}^{+\ (free)}_{k(5,6)} & \mathbf{P}^{+\ (free)}_{k(5,7)} & \mathbf{P}^{+\ (free)}_{k(5,8)} & \mathbf{P}^{+\ (free)}_{k(5,9)} & \mathbf{P}^{+\ (free)}_{k(5,16)} \\ \mathbf{P}^{+\ (free)}_{k(6,1)} & \mathbf{P}^{+\ (free)}_{k(6,2)} & \mathbf{P}^{+\ (free)}_{k(6,3)} & \mathbf{P}^{+\ (free)}_{k(6,4)} & \mathbf{P}^{+\ (free)}_{k(6,5)} & \mathbf{P}^{+\ (free)}_{k(6,6)} & \mathbf{P}^{+\ (free)}_{k(6,7)} & \mathbf{P}^{+\ (free)}_{k(6,8)} & \mathbf{P}^{+\ (free)}_{k(6,9)} & \mathbf{P}^{+\ (free)}_{k(6,16)} \\ \mathbf{P}^{+\ (free)}_{k(7,1)} & \mathbf{P}^{+\ (free)}_{k(7,2)} & \mathbf{P}^{+\ (free)}_{k(7,3)} & \mathbf{P}^{+\ (free)}_{k(7,4)} & \mathbf{P}^{+\ (free)}_{k(7,5)} & \mathbf{P}^{+\ (free)}_{k(7,6)} & \mathbf{P}^{+\ (free)}_{k(7,7)} & \mathbf{P}^{+\ (free)}_{k(7,8)} & \mathbf{P}^{+\ (free)}_{k(7,9)} & \mathbf{P}^{+\ (free)}_{k(7,16)} \\ \mathbf{P}^{+\ (free)}_{k(8,1)} & \mathbf{P}^{+\ (free)}_{k(8,2)} & \mathbf{P}^{+\ (free)}_{k(8,3)} & \mathbf{P}^{+\ (free)}_{k(8,4)} & \mathbf{P}^{+\ (free)}_{k(8,5)} & \mathbf{P}^{+\ (free)}_{k(8,6)} & \mathbf{P}^{+\ (free)}_{k(8,7)} & \mathbf{P}^{+\ (free)}_{k(8,8)} & \mathbf{P}^{+\ (free)}_{k(8,9)} & \mathbf{P}^{+\ (free)}_{k(8,16)} \\ \mathbf{P}^{+\ (free)}_{k(9,1)} & \mathbf{P}^{+\ (free)}_{k(9,2)} & \mathbf{P}^{+\ (free)}_{k(9,3)} & \mathbf{P}^{+\ (free)}_{k(9,4)} & \mathbf{P}^{+\ (free)}_{k(9,5)} & \mathbf{P}^{+\ (free)}_{k(9,6)} & \mathbf{P}^{+\ (free)}_{k(9,7)} & \mathbf{P}^{+\ (free)}_{k(9,8)} & \mathbf{P}^{+\ (free)}_{k(9,9)} & \mathbf{P}^{+\ (free)}_{k(9,16)} \\ \mathbf{P}^{+\ (free)}_{k(16,1)} & \mathbf{P}^{+\ (free)}_{k(16,2)} & \mathbf{P}^{+\ (free)}_{k(16,3)} & \mathbf{P}^{+\ (free)}_{k(16,4)} & \mathbf{P}^{+\ (free)}_{k(16,5)} & \mathbf{P}^{+\ (free)}_{k(16,6)} & \mathbf{P}^{+\ (free)}_{k(16,7)} & \mathbf{P}^{+\ (free)}_{k(16,8)} & \mathbf{P}^{+\ (free)}_{k(16,9)} & \mathbf{P}^{+\ (free)}_{k(16,16)} \end{bmatrix} \tag{98}$$

Therefore, the KF $\delta\mathbf{p}$ covariance will be set to zero. The concept of computing the $\delta\hat{\mathbf{v}}$ from the $\delta\hat{\mathbf{p}}$ is explained in Figure 21. Examining Figure 21, the measurement estimation technique used corresponds to the relationship between position, velocity, the geolocation error of the arbitrary ground feature, and the growth of the velocity

error throughout the measurement epoch. The estimate of the error in position ($\delta\hat{\mathbf{v}} \cdot \Delta t$) growth throughout the measurement epoch can be used to calculate an estimate of the total error in velocity $\delta\hat{\mathbf{v}}$.

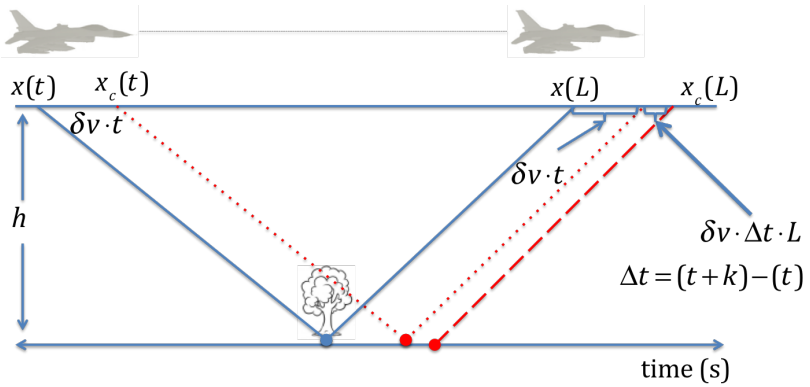

Figure 21. Calculated δv_x Measurement Concept

Inclusion of the navigation state KF originated due to the measurements the navigator was able to take. The benefit of using driftmeter like measurements over time can provide an estimate of the total velocity error rather than just the error in velocity that has increased during tracking of the ground feature.

IV. Results

Research simulation results are presented in the following order: replication of the navigator's use of the driftmeter, replication of the navigator's use of the dirftmeter if correlation would be available, contemporary driftmeter measurement model with the ground feature known and unknown, and a nav. state KF calculating δv_x from δp_x.

4.1 Navigator Replication

In order to validate the approach, a replication of the Navigatior's performance with the driftmeter was constructed. The scripted navigation scenario developed in Section 3.2 was implemented: wings level, constant airspeed, altitude and heading hold. A barometer for altitude measurements, E/O system measurements, and knowledge of time make up the information the Navigator used to calculate a velocity estimate. Use of the barometer constrains the INS altitude error, enabling bearings only measurements of the ground feature to be taken in the x and y directions. Keep in mind that no information about the range of the ground feature can be extracted from the bearings-only measurements. Referencing Equation (63), the states for the system are the navigation state error vector augmented with the biases in the accelerometers, gyroscopes, and the barometric altitude sensor bias. The replication of driftmeter performance measurement model can be seen in Equation (99), where the velocity in the x direction, altitude, and baro bias are observable.

$$\mathbf{H}_k = \begin{bmatrix} 0 & 1 & 0 & 0 & 0 & 0 & 0 & 0 & 0 & 0 & 0 & 0 & 0 & 0 & 0 & 0 \\ 0 & 0 & 1 & 0 & 0 & 0 & 0 & 0 & 0 & 0 & 0 & 0 & 0 & 0 & 0 & -1 \end{bmatrix} \tag{99}$$

Figure 22 shows the results of the simulation with tracking of a ground feature at

half time (30 min) into the flight duration. At the end of the measurement epoch, the INS is reset by way of subtracting the Kalman filter navigation state error estimates from the free running INS navigation state measurements. The Kalman filter is initialized with the free INS navigation state error covariance values, ignoring cross-correlation terms which are set to zero. Knowing the ground feature is stationary, tracking it throughout the duration of the measurement epoch, the filter is able to estimate the velocity error from the system output through observability. However, errors in position are unobservable. Conceptually, accumulated position error prior to measurement availability and estimation update cannot be corrected purely with a relative update.

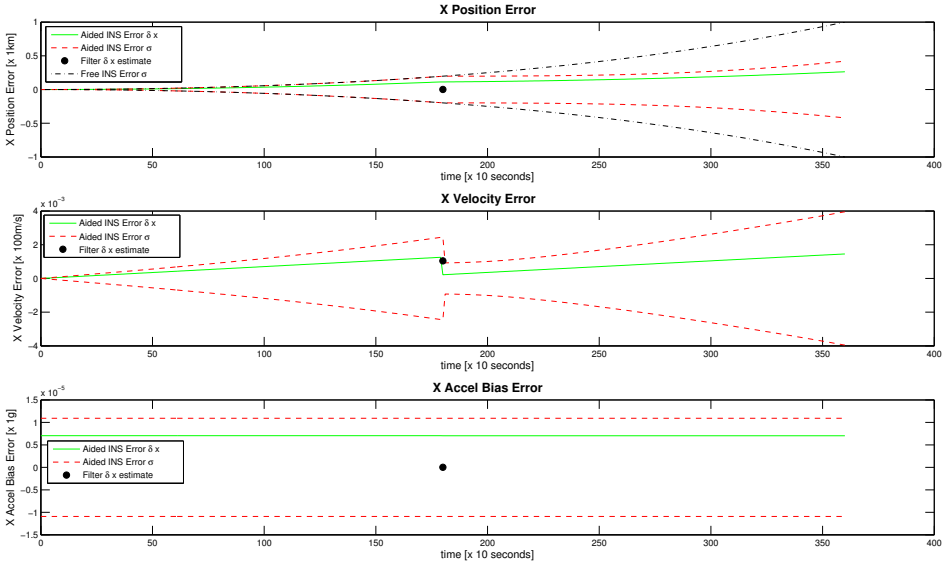

Figure 22. X Pos, Vel, Accel Bias Error - Full Channel Navigator Replication (KF initialized with NO cross-correlation)

When analyzing the observability of the system, rank deficiency indicates the navigation state error is not fully observable [11]. In a case where the INS error dynamics are known, initializing the Kalman filter at half time with the free running INS navigation state estimation error covariance can provide observability through

correlation. Specifically, $\mathbf{P}_0^+$ of the Kalman filter is set to $\mathbf{P}_k$ from the free INS. Below, Figure 23 shows the results using observability through correlation.

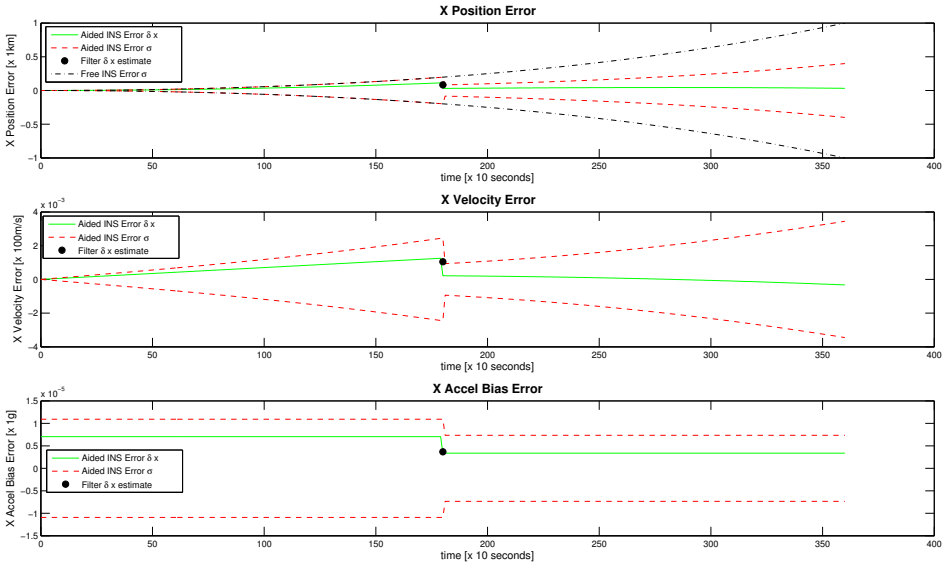

Figure 23. X Pos, Vel, Accel Bias Error - Full Channel Navigator Replication (KF initialized with cross-correlation)

As opposed to the Kalman filter initialized with zero cross-correlation, the results using correct cross-correlation yield improvements in estimation observability. Specifically, x position and x accelerometer bias error estimates are significantly improved compared to the data driven estimates obtained without observability through correlation. With a good estimate of the residual accelerometer bias courtesy of correlation, the remaining error propagation model of the INS error will be significantly improved as the accelerometer bias strongly affects the velocity and position error.

Thus, knowledge of the INS navigation state error dynamics allows the incorporation of state cross-covariance based on the INS error equation propagation. Initializing the Kalman filter with the full free INS covariance, yields a x position estimate coinciding with the velocity measurement available to the Kalman filter. At the conclusion of the 1 hour flight, a 60% reduction in error covariance is realized while eliminating

a large portion of the free INS error.

Verified as a proof of concept in simulation, tasking the pilot to track a stationary ground feature can provide significant position error improvements (60%) without knowing the position of the ground feature. However, it is important to note, observability through correlation is possible because the flight condition prior to the measurement epoch is known and in this case it is the same flight condition during the measurement epoch.

Implementing the measurement model developed in Section 3.3 demonstrates a higher fidelity simulation of the aiding action available with bearings-only measurements. Consider the automation of the World War II navigator's function using contemporary technology to significantly reduce the human and instrumentation errors.

4.2 INS Error Model Robustness to Axis Acceleration

The robustness of the INS error model was inspected in order to validate the simplified flight conditions pursued in Section 4.3. Referring to Section 3.3, the INS error model was tested with acceleration inputs in the a_x axis prior to and following and INS aiding session. During the INS aiding session only, wings level flight conditions annotated in Section 3.2 are used.

Table 4 shows the difference in position error if acceleration inputs prior to flight exist vs a steady-state flight condition. Taking the difference between the resultant position error in the x direction at the end of the 1 hour flight was used as a robustness test of the INS error model. Equation (100) shows the difference in the position error in the x direction comparing the INS error model with steady-state dynamics and with an input sinusoidal acceleration input.

$$\Delta x = x_{acceleration} - x_{steady-state} \tag{100}$$

The values are non-dimensionalized when compared and therefore, the equivalent units are meters. As the frequency of the sine wave increases, the acceleration inputs appear to cancel out over the course of the flight which is a limitation of this analysis. Hence, the empirical testing of a reasonable frequency to simulate an acceleration flight profile. Even with increased magnitude, up to $1g$ of acceleration force, the largest difference in final position error does not exceed 20 m.

Table 4. INS Position Error Difference Δx Results

	$\omega(\frac{rad}{s})$				
$\frac{a}{g}$		**0.005**	**0.05**	**0.5**	**1**
	0.2	4	0.04	−0.002	0.004
	0.4	7	0.07	−0.006	0.006
	0.6	11	0.12	−0.009	0.008
	0.8	15	0.14	−0.013	0.012
	1.0	19	0.18	−0.016	0.015

4.3 Contemporary Driftmeter

Consider the same flight condition outlined in Section 3.2. Simulations were initially run for a case where the position of the ground feature is known at the beginning of the aiding session to validate the measurement model. Then geolocation of the ground feature was calculated using the INS and E/O system measurements which are corrupted with $\delta\mathbf{x}$ from the INS and δx_f and δy_f from the E/O system.

With the position of the ground feature known, the filter is able to estimate the INS velocity error by taking measurements over time to a stationary ground feature.

In the measurements taken throughout the duration of the epoch, the ground feature is geolocated with geometry using the INS output and the E/O system. Using the known location of the ground feature is similar to the practices of IP inertial system updates in terms of an absolute update. Testing with a known ground feature location given to the KF at time $k = 0$ served as a basis for validating the measurement model.

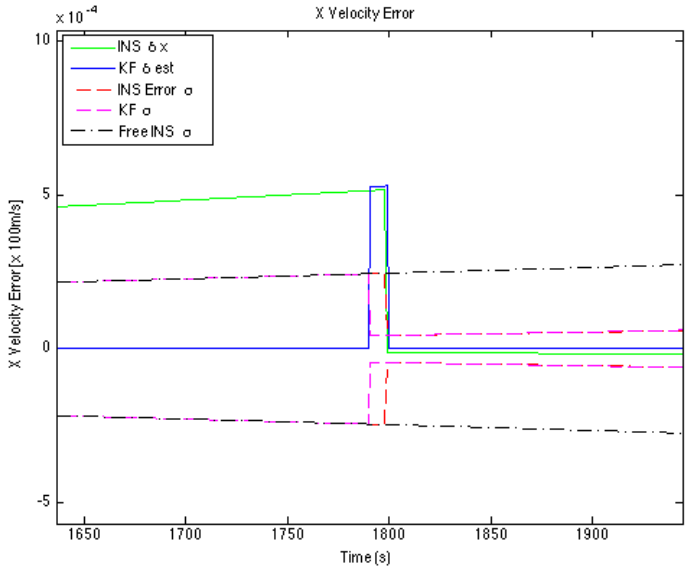

Figure 24. X Velocity Error - Ground Feature Location Known

Figure 25 shows the geolocation track calculated using the INS and the E/O system. A strong relationship between the altitude error δz and the ability to correctly geolocate the stationary ground feature was observed. Geolocation of the ground feature was done eliminating altitude error, eliminating angular error, and with only the E/O system error for comparison. Also, the ground feature geolocation throughout the epoch is distributed around the initial geolocation due to the accumulation of errors at the beginning of the epoch. The drift of the ground feature location throughout the epoch is attributed to the increase in $\delta\mathbf{x}$, $\delta\boldsymbol{\psi}$, and the E/O system pixel errors observed during the INS aiding session.

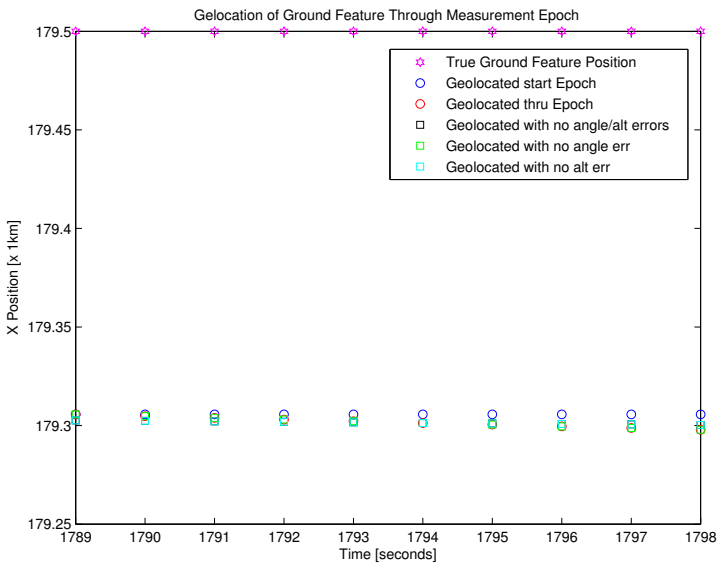

Figure 25. Ground Feature Geolocation Track - Ground Feature Location Known

Geolocation of an unknown ground feature at the beginning of the measurement epoch proves to only provide an estimate of the accumulation of the error during the INS aiding session. This is due to the presence of relatively the same errors used to geolocate the ground feature at $l = 0$ and throughout the epoch at $l = 1, 2, ..., L$. Figure 26 shows the weak estimation, with a zoomed in view in Figure 27, of the total δv_x since the beginning of the flight.

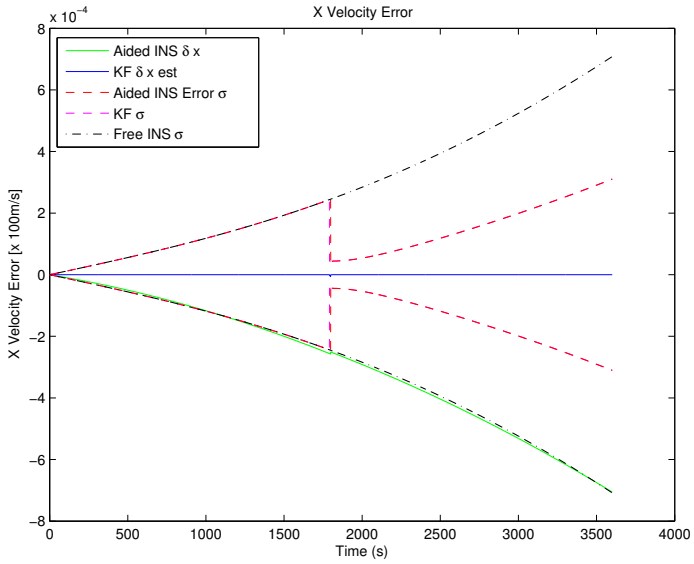

Figure 26. X Velocity Error - Ground Feature Location Unknown

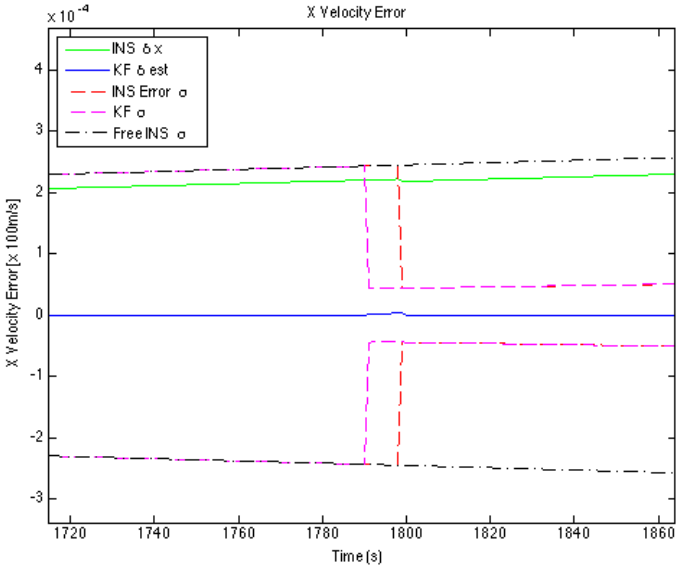

Figure 27. X Velocity Error - Ground Feature Location Unknown - Zoomed In

With a weak estimate in velocity error, $\delta\mathbf{v}$, the estimation of the accelerometer bias is proportionally weak. A good estimate of the accelerometer bias would have been used to decrease the accumulation of INS error after the INS aiding session in Figure 28.

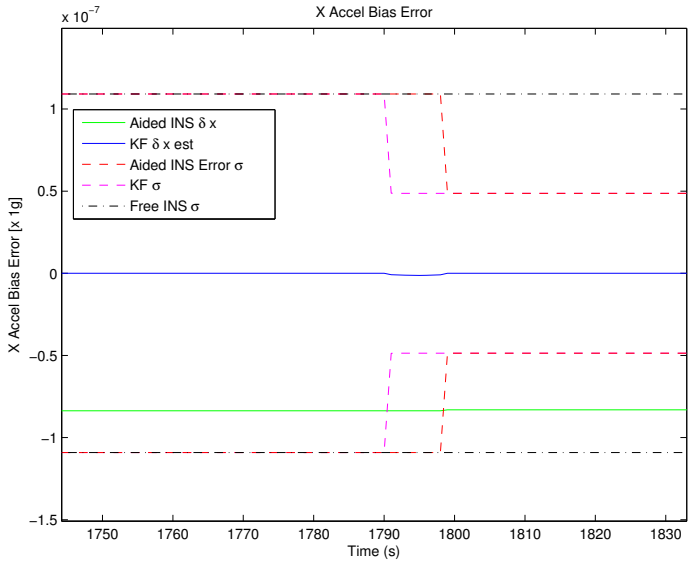

Figure 28. X Accelerometer Bias Error - Ground Feature Location Unknown - Zoomed In

The ground track of the geolocated ground feature still follows the relationship dependency on δz. Which validates the use of the barometric sensor for altitude aiding to constrain the errors in the z channel.

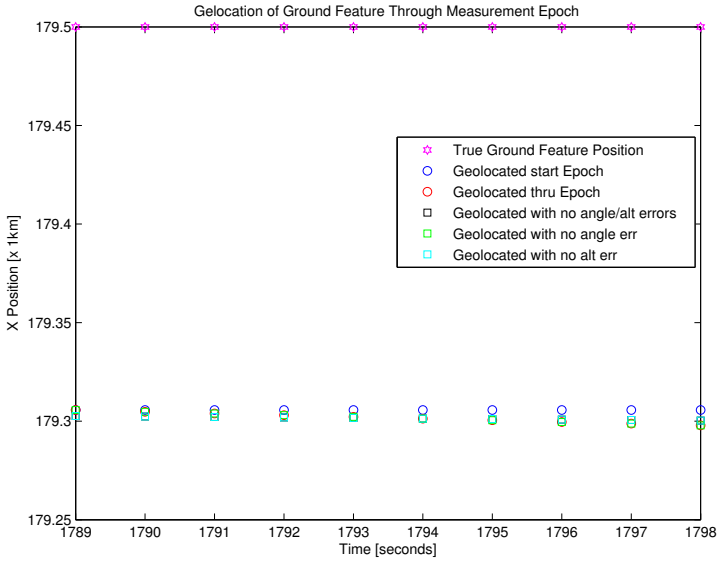

Figure 29. Ground Feature Geolocation Track - Ground Feature Location Unknown

4.4 Navigation State Kalman Filter

The navigation state KF attempts to investigate the possibility the system is over modeled for the measurements available. From an observability perspective, reduction of augmented correlated states will enhance the observability of the system. Presented in this section are the results of the implementation of a navigation state KF.

The results show that an estimate in velocity does more than just estimate the growth of velocity error during the measurement epoch, shown in Figure 30. Therefore, using the estimate in velocity error, the INS is reset which in turn positively impacts the growth of error in position, shown in Figure 31.

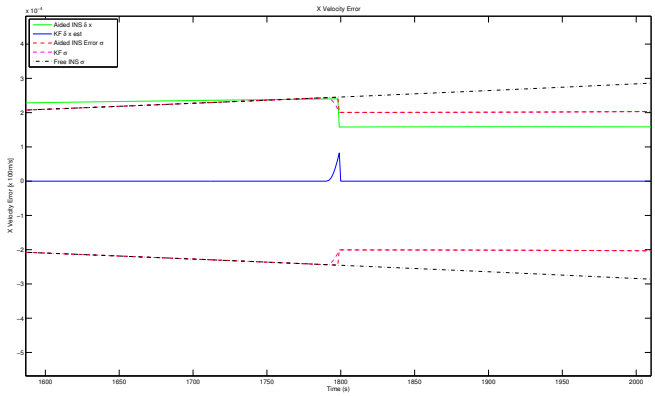

Figure 30. Reduced State KF with calculated δv_x - X Velocity Error

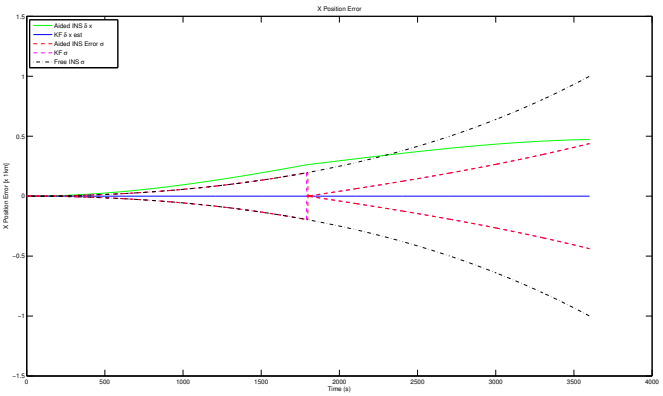

Figure 31. Reduced State KF with calculated δv_x - X Position Error

V. Conclusion

The research performed, investigating a bearings-only INS aiding method with an E/O system has continued the push for inertial navigation research. Reliance on GPS systems is becoming an obvious concern in many applications including the military. Research focusing on passive, self contained navigation sensors is paramount. Navigators in World War two were not afforded the technology available today, but were still able to navigate via dead reckoning with a driftmeter. Therefore, the investigation into what the driftmeter actually brought to the table is warranted. Realizing the human and component errors corrupting the navigator's use of the driftmeter, the question this research focused on is can we use driftmeter principles with contemporary technology to aid a navigation grade INS. Simulations were developed to replicate the navigator's use of the driftmeter during the course of a $1hr$ flight. The results were evaluated indicating the navigator was able to calculate his error in velocity well. Understanding the relationship between position and velocity presented a segue to the geolocation of an arbitrary ground feature at the beginning of a measurement epoch and subsequently geolocating the ground feature throughout the epoch. The growth of the error throughout the epoch can be used to back out an estimate of the INS error in velocity, δv.

5.1 Conclusions - Contributions

Simulation results presented in Chapter IV are not of the precision navigation performance of a consumer grade GPS standard positioning source [7]. But the value added comes in the form of the ability to generate an estimate of the total error in velocity positively impacts the remaining growth of the INS errors. The ability to implement this technique with current operational technology with little integration

makes the approach advantageous for flight testing.

5.2 Recommendations for Future Work

A robust analysis on the impact of trajectory on the INS errors to validate the simplified error equation model used to propagate the $free$ INS would be beneficial from a verification standpoint. Even though the purpose of error models are to eliminate the dependency on high frequency component dynamics, the modeling error associated with dynamic flight conditions while running steady-state INS error equations should be tested.

It was discovered the high dependency the z channel had on the geolocation of the ground feature due to geometry. Understanding the GDOP constraints in the flight scenario and the operating limitations of this approach would be valuable. The GDOP is driven by the error in altitude, aircraft velocity, and time. Evaluating the performance of E/O systems and determining a cutline for the E/O system measurement uncertainty needed to constructively aid a navigation grade inertial system. Testing the limits of the E/O system was not in the scope of this initial contemporary driftmeter replication.

Increasing the fidelity of a simulation model is always an avenue for future work. The current implementation of INS error sources is strictly the accelerometer bias and the gyroscope bias. Including the drift and scale factor errors would increase the fidelity of the INS error model but are not a necessity for an understanding of the how bearings-only measurements over time can aid the INS.

Bibliography

1. Bar-Itzhack, Itzhack Y and N Berman. "Control theoretic approach to inertial navigation systems". *Journal of Guidance, Control, and Dynamics*, 11(3):237–245, 1988.

2. Boie, Robert A. and Ingemar J. Cox. "An analysis of camera noise". *IEEE Transactions on Pattern Analysis and Machine Intelligence*, 14(6):671–674, 1992.

3. Britting, Kenneth R. *Inertial navigation systems analysis*. 2010.

4. Command, USAF Air Training. "Air Navigation", October 1971.

5. Decker, B LOUIS. *World geodetic system 1984*. Technical report, DTIC Document, 1986.

6. Floreano, Dario and Claudio Mattiussi. *Bio-inspired artificial intelligence: theories, methods, and technologies*. MIT press, 2008.

7. Gov, GPS. "GPS Standard Positioning Service (SPS) Performance Standard". *GPS. Gov Website. Accessed January*, 4, 2015.

8. Hwang, Robert Grover Brown Patrick YC and Robert Grover Brown. "Introduction to random signals and applied Kalman filtering". *John Wiley & Sons, Inc,*, 5:39–45, 1997.

9. Inc., Honeywell International. "AM-250 Barometric Altimeter", 12 2008. URL `http://www51.honeywell.com/aero/common/documents/myaerospacecatalog-documents/BA_brochures-documents/AM-250_Baro_Altimeter.pdf`. Honeywell AM-250 Barometric Altimeter Datasheet [Accessed: November 2014].

10. Inc., Honeywell International. "HG9900 IMU", 9 2009. URL `http://aerospace.honeywell.com/~/media/Military\%20IMU\%20Brochure\%20PDF/HG9900\%20Nav-Grade\%20IMU.ashx`. Honeywell HG9900 IMU Datasheet [Accessed: November 2014].

11. Katsuhiko, Ogata. "Modern control engineering". 684–688, 2010.

12. Lintereur, Louis Josesph. *Optimal test trajectories for calibrating inertial systems*. Ph.D. thesis, Massachusetts Institute of Technology, 1996.

13. Magree, Daniel and Eric N Johnson. "A Monocular Vision-aided Inertial Navigation System with Improved Numerical Stability".

14. Maybeck, Peter S. *Stochastic models, estimation, and control*, volume 1. Academic press, 1982.

15. Pachter, M. and A. Porter. "Bearings-only measurements for INS aiding: the three-dimensional case". *American Control Conference, 2004. Proceedings of the 2004*, volume 6, 5363–5368 vol.6. June 2004. ISSN 0743-1619.

16. Pachter, Meir, Alec Porter, and Murat Polat. "Aiding Using Bearings-Only Measurements of an Unknown Ground Object". *Institute Of Navigation*, 13(1):1–20, 7 2006. "Reprinted in the ION Red Book Vol 7, selected papers on integrated systems".

17. Quarmyne, James O. *Inertial Navigation System Aiding Using Vision*. Technical report, DTIC Document, 2013.

18. Relyea, Andrew L. *Covariance Analysis of Vision Aided Navigation by Bootstrapping*. Technical report, DTIC Document, 2012.

19. Scaramuzza, Davide and Friedrich Fraundorfer. "Visual odometry [tutorial]". *Robotics & Automation Magazine, IEEE*, 18(4):80–92, 2011.

20. Schwartz, General Norton A. "The Challenge of Central Banking in a Democratic Society", 1 2010. URL `http://www.ifpafletcherconference.com/2010/transcripts/Gen_Schwartz_Opening-Keynote_Jan20.pdf`. Keynote address by Chief of Staff of the United States Air Force [Accessed: August 2014].

21. Titterton, David and John L Weston. *Strapdown inertial navigation technology*, volume 17. IET, 2004.

22. Tuma, Allan D. *Automated Driftmeter Fused with Inertial Navigation*. Technical report, DTIC Document, 2014.

23. Veth, Michael J. *Fusion of imaging and inertial sensors for navigation*. Technical report, DTIC Document, 2006.

24. Veth, Mike and John Raquet. *Fusion of low-cost imaging and inertial sensors for navigation*. Technical report, DTIC Document, 2007.

25. Zhang, Zhengyou. "Flexible camera calibration by viewing a plane from unknown orientations". *Computer Vision, 1999. The Proceedings of the Seventh IEEE International Conference on*, volume 1, 666–673. IEEE, 1999.

List of Acronyms

AFIT Air Force Institute of Technology

ANT Autonomy and Navigation Technology

CCD Charge Coupled Device

CDF Cumulative Distribution Function

CENSURE Center Surround Extremas

DCM Direction Cosine Matrix

ECEF Earth Centered Earth Fixed

EKF Extended Kalman Filter

ENU East - North - Up

E/O Electro-Optical

FOGM First Order Gaussian Markov

GDOP Geometric Dilution of Precision

GNSS Global Navigation Satellite System

GPS Global Positioning System

IMU Inertial Measurement Unit

INS Inertial Navigation System

IP Initial Point

KF Kalman Filter

LHS Left Hand Side

LOS Line of Sight

MEMS Micro-Electrical Mechanical Sensors

MMSE Minimum Mean Squared Estimator

PDF Probability Distribution Function

PVA Position Velocity Attitude

RF Radio Frequency

RHS Right Hand Side

SIFT Scale Invariant Feature Transformation

SLAM Simultaneous Localization and Mapping

SNR Signal-to-Noise Ratio

SURF Speeded Up Robust Transformation

REPORT DOCUMENTATION PAGE

Form Approved
OMB No. 0704–0188

1. REPORT DATE *(DD–MM–YYYY)*	2. REPORT TYPE	3. DATES COVERED *(From — To)*
26–03–2015	Master's Thesis	Sept 2013 — Mar 2015

4. TITLE AND SUBTITLE

Pilot Assisted Inertial Navigation System Aiding Using Bearings-Only Measurements Taken Over Time

5a. CONTRACT NUMBER

5b. GRANT NUMBER

5c. PROGRAM ELEMENT NUMBER

6. AUTHOR(S)

Mirabile, Anthony T, 1st Lt

5d. PROJECT NUMBER

15G454D

5e. TASK NUMBER

5f. WORK UNIT NUMBER

7. PERFORMING ORGANIZATION NAME(S) AND ADDRESS(ES)

Air Force Institute of Technology
Graduate School of Engineering and Management (AFIT/EN)
2950 Hobson Way
WPAFB OH 45433-7765

8. PERFORMING ORGANIZATION REPORT NUMBER

AFIT-ENG-MS-15-M-015

9. SPONSORING / MONITORING AGENCY NAME(S) AND ADDRESS(ES)

Air Force Research Laboratory
Attn: Dr. Stewart DeVilbiss
2241 Avonics Dr. bldg 620
WPAFB, OH 45433
Phone: (312)798-4413
Email: stewart.devilbiss.1@us.af.mil; stewart.devilbiss@afit.edu

10. SPONSOR/MONITOR'S ACRONYM(S)

AFRL/RYWN

11. SPONSOR/MONITOR'S REPORT NUMBER(S)

12. DISTRIBUTION / AVAILABILITY STATEMENT

DISTRIBUTION STATEMENT A:
APPROVED FOR PUBLIC RELEASE; DISTRIBUTION UNLIMITED.

13. SUPPLEMENTARY NOTES

This work is declared a work of the U.S. Government and is not subject to copyright protection in the United States.

14. ABSTRACT

The objective of this work is to develop an alternative INS aiding source other than the GPS, while preserving the autonomy of the integrated navigation system. It is proposed to develop a modernized method of aerial navigation using driftmeter measurements from an E/O system for ground feature tracking, and an independent altitude sensor in conjunction with the INS. The pilot will track a ground feature with the E/O system, while the aircraft is on autopilot holding constant airspeed, altitude, and heading during an INS aiding session. The ground feature measurements from the E/O system and the INS output form measurements provided to a linear KF running on the navigation computer to accomplish the INS aiding action. Aiding the INS will be periodically repeated as operationally permissible under pilot discretion. Little to no modeling error will be present when implementing the linear Kalman filter, indicating the strength of the INS aiding action will be exclusively determined by the prevailing degree of observability.

15. SUBJECT TERMS

Vision-Aided Inertial Navigation, Driftmeter, Targeting Pod, Kalman Filter, Simulation, Bearing Measurements

16. SECURITY CLASSIFICATION OF:			17. LIMITATION OF ABSTRACT	18. NUMBER OF PAGES	19a. NAME OF RESPONSIBLE PERSON
a. REPORT	b. ABSTRACT	c. THIS PAGE			Dr. Meir Pachter, AFIT/ENG
U	U	U	U	105	19b. TELEPHONE NUMBER *(include area code)* (937) 255-3636, x7247; meir.pachter@afit.edu